J. Fluid Mech. (1989), *vol.* 205, *pp.* 263–295
Printed in Great Britain

Merger and cancellation of strained vortices

By JAMES D. BUNTINE† AND D. I. PULLIN
Department of Mechanical Engineering, University of Queensland,
St Lucia, 4067 Queensland, Australia

(Received 4 November 1988 and in revised form 20 February 1989)

We study numerically the behaviour of and interaction between Burgers vortices – a known equilibrium solution to the Navier–Stokes equations which incorporates a balance between viscous diffusion and strain intensification of vorticity. A hybrid spectral/finite-difference method is employed to solve the Navier–Stokes equations in vorticity–stream function form for a unidirectional vorticity field on an infinite domain in the presence of a uniform three-dimensional strain field, one principal axis of which is parallel to the vorticity. Merging of two strained vortices is studied over a range of Reynolds numbers $Re = \Gamma/2\pi\nu = 10$–1280, and the results are used to calculate an energy spectrum for three-dimensional, homogeneous turbulence. The cancellation of two strained vortices with opposing circulation is investigated for Reynolds numbers $Re = \Gamma_0/2\pi\nu = 0.1$–$160$ (Γ_0 is the circulation about one vortex), over a range of strain rates in the direction parallel to the line joining the vortex centres. A solution of the Navier–Stokes equations describing vorticity cancellation in the strain-induced collision of vortex layers (Kambe 1984) is used to estimate the asymptotic, timewise decay of circulation for each vortex. Good agreement with the present numerical results is obtained. Vortex core pressures calculated during the cancellation event are compared to a simple analytical model based on Moore & Saffman (1971).

1. Introduction

Central to the processes believed to occur in turbulence is the idea of the compact vorticity field and the transport of energy between scales of motion provided by the action of vortex stretching. For this reason, the behaviour of finite regions of vorticity in an inviscid fluid has received considerable attention. Omitting the viscous terms in the Navier–Stokes equations gives the much-studied inviscid Euler equations. Moore & Saffman (1971) found steady solutions of the incompressible Euler equations for finite-area, constant-strength vortices in an inviscid fluid subjected to a two-dimensional, irrotational strain field. Kida (1981) and Neu (1984*a*) have extended this to unsteady flow and a three-dimensional strain which stretches vortex lines. Deem & Zabusky (1978) developed the contour-dynamics approach to study the interaction of finite-area vortices of like signs. Jacobs & Pullin (1985) combined both the interaction of finite-area vortices and a three-dimensional strain field to model processes (in the inviscid limit) believed to occur in the transfer of energy between flow structures at very high Reynolds numbers.

Viscosity complicates the solution of the Navier–Stokes equations for vorticity–strain field interaction at high Reynolds numbers owing to the necessity to

† Present address: Applied Mathematics 217-50, California Institute of Technology, Pasadena, CA 91125, USA.

resolve dissipation scales, and limited results are available. Lundgren (1982) used an asymptotic analysis of viscous spiral vortices in a stretching, axisymmetric strain field to obtain an energy spectrum for homogeneous turbulence, while Kambe (1984) found an analytical solution describing the cancellation of vortex layers embedded in three-dimensional strain. Vortex interactions in an unstrained flow have been studied in detail by Melander, McWilliams & Zabusky (1987) who considered very high-Reynolds-number behaviour of vortices through the introduction of a hyperviscosity term used to suppress small-scale motions.

An exact solution of the Navier–Stokes equations (Burgers 1948) describes a steady equilibrium between the action of viscous diffusion and vortex intensification caused by a strain field with one principal axis aligned with the vorticity. The solutions take the form of a cylindrical vortex when the strain field is circularly symmetric and a vortex layer when the strain field is planar. Robinson & Saffman (1984) extended Burgers' result to vortices in a non-axisymmetric strain field.

Townsend (1951) used ensembles of stretched vortices to model the fine scales of turbulence. In studying the dynamics of strained streamwise vortices in the mixing layer, Lin & Corcos (1984) (see also Corcos & Lin 1984; Corcos & Sherman 1984; Neu 1984*b*) observed the formation of compact, nearly axisymmetric vortices embedded in the strain field of the primary vortex array. Perry & Chong (1982) obtained predictions of mean and turbulence flow properties for wall-bounded flows using hierarchies of strained horseshoe vortices. In numerical solutions of three-dimensional Navier–Stokes turbulence, Ashurst *et al.* (1987) find alignment between the vorticity and one principal axis of the local strain. Vortex stretching appears to play an important role in vortex reconnection events of the type studied experimentally by Schatzle (1987) (see also related numerical simulations by Leonard & Winckelmans 1988; Meiron, Orszag & Shelly 1988). Siggia & Pumir (1988) find extremely large self-stretching of a vortex tube following pairing of tube segments with antiparallel circulation, suggesting complex local processes involving competition between vortex stretching, viscous cancellation of vorticity, and inertia.

In the present paper we consider separately the merger of, and the mutual cancellation of, strained vortex pairs in a viscous fluid. Our aim is to study the properties of these fundamental types of vortex interaction and to elucidate their possible role in some aspects of turbulence mechanics. Section 2 outlines the equations governing the behaviour of an initial distribution of vorticity subjected to a three-dimensional, uniform (possibly time-varying) strain field with one principal axis aligned with the vorticity, in an infinite two-dimensional domain. A solution method is given in §3 which incorporates a hybrid spectral/fourth-order finite-difference scheme to solve the governing equations mapped onto a finite domain. This has the advantage of eliminating the need for periodic or approximate boundary conditions required when a finite computational region is employed.

In §4 we examine the merging of two Burgers vortices at Reynolds numbers ranging from $Re = \Gamma/2\pi\nu = 1$–1280. By replacing an ensemble average with a time average over an individual merging event, the energy spectrum of a homogeneous turbulence field comprising pairing Burgers vortices is calculated. Cancellation of two Burgers vortices with equal strength but opposite sign is considered in §5, where the dependence is explored of the evolution, and in particular the vortex cancellation time, on both Reynolds number ($Re = 0.1$–160) and compressive strain in the direction joining the vortex cores.

2. Problem definition

2.1. *Governing equations*

Both cylindrical polar and Cartesian coordinate systems are used. The cylindrical coordinates and their corresponding unit vectors are (r, θ, z) and $(\hat{\boldsymbol{r}}, \hat{\boldsymbol{\theta}}, \hat{\boldsymbol{k}})$ respectively. For Cartesian coordinates, they are (x, y, z) and $(\hat{\boldsymbol{i}}, \hat{\boldsymbol{j}}, \hat{\boldsymbol{k}})$. These systems are related through,

$$x = r\cos\theta, \quad y = r\sin\theta, \tag{2.1a, b}$$

All flows considered possess unidirectional vorticity

$$\boldsymbol{\omega} = \omega(r, \theta)\,\hat{\boldsymbol{k}}. \tag{2.2}$$

The vorticity is subjected to a three-dimensional straining flow with one principal axis of strain aligned with $\boldsymbol{\omega}$. The full velocity field is written as

$$\boldsymbol{u}(r, \theta, z, t) = \boldsymbol{v}(r, \theta, t) + \boldsymbol{u}_{\mathrm{s}}, \tag{2.3}$$

where the first term is the vortex-induced velocity which lies entirely in the (r, θ) (or (x, y))-plane and the second term, $\boldsymbol{u}_{\mathrm{s}}$, is the uniform strain field

$$\boldsymbol{u}_{\mathrm{s}} = -\beta(t)\,x\hat{\boldsymbol{i}} + [\beta(t) - \gamma(t)]\,y\hat{\boldsymbol{j}} + \gamma(t)\,z\hat{\boldsymbol{k}}, \tag{2.4}$$

where $\beta(t)$ and $\gamma(t)$ are strain rates. They are assumed to be known functions of time.

Substituting (2.2)–(2.4) into the vorticity transport equation gives a simplified form

$$\frac{\partial \omega}{\partial t} + \boldsymbol{\nabla}\cdot(\boldsymbol{u}\omega) = \gamma\omega + \nu\nabla^2\omega. \tag{2.5}$$

Since the fluid is incompressible, a stream function $\psi(r, \theta, t)$ associated with the $\boldsymbol{v}$-motion can be defined, where

$$\nabla^2\psi = -\omega, \tag{2.6}$$

$$\boldsymbol{v} = \boldsymbol{\nabla} \wedge (\psi\boldsymbol{k}). \tag{2.7}$$

Most subsequent discussion will deal with the equations given above in cylindrical coordinates. The strain field, $\boldsymbol{u}_{\mathrm{s}}$ is then

$$\boldsymbol{u}_{\mathrm{s}} = -\tfrac{1}{2}r[(2\beta - \gamma)\cos 2\theta + \gamma]\,\hat{\boldsymbol{r}} + \tfrac{1}{2}r(2\beta - \gamma)\sin 2\theta\hat{\boldsymbol{\theta}} + \gamma z\hat{\boldsymbol{k}}, \tag{2.8}$$

and the velocity associated with the vorticity field is

$$v_r = \frac{1}{r}\frac{\partial \psi}{\partial \theta}, \quad v_\theta = -\frac{\partial \psi}{\partial r}, \tag{2.9}$$

where

$$\boldsymbol{v} = v_r\hat{\boldsymbol{r}} + v_\theta\hat{\boldsymbol{\theta}}.$$

Hence the vorticity transport equation becomes

$$\frac{\partial \omega}{\partial t} + u_r\frac{\partial \omega}{\partial r} + \frac{1}{r}u_\theta\frac{\partial \omega}{\partial \theta} = \gamma\omega + \frac{\nu}{r}\left\{\frac{\partial}{\partial r}\left(r\frac{\partial \omega}{\partial r}\right) + \frac{1}{r}\frac{\partial^2 \omega}{\partial \theta^2}\right\}. \tag{2.10}$$

The components of (2.3) are

$$u_r = v_r - \tfrac{1}{2}r[(2\beta - \gamma)\cos 2\theta + \gamma], \tag{2.11}$$

$$u_\theta = v_\theta + \tfrac{1}{2}r(2\beta - \gamma)\sin 2\theta, \tag{2.12}$$

while the Poisson equation is

$$\frac{1}{r}\frac{\partial}{\partial r}\left(r\frac{\partial \psi}{\partial r}\right)+\frac{1}{r^2}\frac{\partial^2 \psi}{\partial \theta^2}=-\omega. \tag{2.13}$$

The problem is to solve (2.10)–(2.13) numerically with given $\gamma(t)$, $\beta(t)$ and subject to initial and boundary conditions on the vorticity field given by

$$\omega(r,\theta,t=0) \quad \text{given}, \tag{2.14}$$

$$\omega(r\to\infty,\theta,t)\to 0, \quad t\geqslant 0. \tag{2.15}$$

Specific initial conditions will consist of several (two) concentrations of vorticity which may initially be identified as separate 'vortices'. Flows considered will include those for which the global (conserved) circulation,

$$\Gamma=\int_0^{\infty}\int_0^{2\pi}\omega(r,\theta,t)\,r\,\mathrm{d}r\,\mathrm{d}\theta=\text{constant}, \tag{2.16}$$

may be finite or zero.

If it is assumed that the vorticity decays like a Burgers vortex at large distances from the origin (i.e. $\omega\sim\exp(-kr^2)$, as $r\to\infty$, where k is some constant), the solution of the Poisson equation as $r\to\infty$, gives the leading-order terms for the stream function as

$$\psi(r,\theta,t)=\frac{\Gamma}{2\pi}\ln(r)+\frac{1}{2\pi r}[A\cos\theta+B\sin\theta]+O(1/r^2), \tag{2.17}$$

where A and B are constants. The first term contains the effect of finite circulation, and the second term is a vortex dipole.

2.2. *The axisymmetric Burgers vortex*

When $\beta=\frac{1}{2}\gamma$, the strain field is axisymmetric. Burgers (1948) obtained a steady, analytical solution to (2.10)–(2.13), for this case if $\Gamma>0$ and $\gamma=$ constant:

$$\omega(r,\theta,t)=\frac{\Gamma\gamma}{4\pi\nu}\mathrm{e}^{-\gamma r^2/4\nu}. \tag{2.18}$$

Equation (2.17) reduces here to

$$\psi\to\frac{\Gamma}{2\pi}\ln(r)+o(\mathrm{e}^{-r^2}) \quad \text{as } r\to\infty. \tag{2.19}$$

This solution represents a balance between the action of viscous diffusion and vorticity intensification due to the stretching strain field. A radius for the Burgers vortex may be defined as

$$a_{\mathrm{BV}}=\left(\frac{4\nu}{\gamma}\right)^{\frac{1}{2}}. \tag{2.20}$$

2.3. *Equivalent two-dimensional flow*

The stretched vortex problem defined in §2.1 may be mapped to an equivalent fully two-dimensional flow using the rescaling transformation (Batchelor 1967; Lundgren 1982; Giga & Kambe 1987)

$$A(t) = \int_0^t \gamma(t')\,\mathrm{d}t', \tag{2.21}$$

$$\xi = r\,\mathrm{e}^{\frac{1}{2}A}, \tag{2.22}$$

$$\tau = \int_0^t \mathrm{e}^{A(t')}\,\mathrm{d}t', \tag{2.23}$$

$$\Omega(\xi, \theta, \tau) = \omega(r, \theta, t)\,\mathrm{e}^{-A(t)}, \tag{2.24}$$

where ξ is the rescaled radial coordinate, τ is a stretched time variable and Ω is the corresponding vorticity in this new system. Applying (2.21)–(2.24) to (2.10) gives

$$\frac{\partial \Omega}{\partial t} + U_r \frac{\partial \Omega}{\partial \xi} + U_\theta \frac{1}{\xi}\frac{\partial \Omega}{\partial \theta} = \nu\left(\frac{\partial^2 \Omega}{\partial \xi^2} + \frac{1}{\xi}\frac{\partial \Omega}{\partial \xi} + \frac{1}{\xi^2}\frac{\partial^2 \Omega}{\partial \theta^2}\right) \tag{2.25a}$$

$$U_r = V_r - \mathrm{e}^{-A}\tfrac{1}{2}\xi(-\beta + \tfrac{1}{2}\gamma)\cos 2\theta, \tag{2.25b}$$

$$U_\theta = V_\theta + \mathrm{e}^{-A}\tfrac{1}{2}\xi(-\beta + \tfrac{1}{2}\gamma)\sin 2\theta, \tag{2.25c}$$

where $(V_r, V_\theta) = (v_r, v_\theta)\,\mathrm{e}^{-A/2}$ are the rescaled velocity components associated with the vorticity. Equation (2.25*a*) is a two-dimensional vorticity transport equation describing a vortex motion with vorticity

$$\Omega = \frac{1}{\xi}\left[\frac{\partial(\xi V_\theta)}{\partial \xi} - \frac{\partial V_r}{\partial \theta}\right]$$

which is subject to a two-dimensional, time-dependent uniform strain. When the strain is axisymmetric ($\beta = \frac{1}{2}\gamma$), U_s vanishes giving strictly two-dimensional flow with zero fluid velocity at $r = \infty$.

2.4. *Scaling*

Throughout this paper an overbar will be used to denote dimensional quantities. All other variables can be considered non-dimensional unless otherwise specified. A Reynolds number is defined as,

$$Re = \frac{\bar{\Gamma}}{2\pi\bar{\nu}}. \tag{2.26}$$

We set the length and time scales as

$$L = (4\bar{\nu}/\bar{\gamma})^{\frac{1}{2}}, \tag{2.27}$$

$$T = 4\bar{\gamma}^{-1}. \tag{2.28}$$

The scalings ensure that an equilibrium Burgers vortex will have unit radius, for all values of circulation. Also the stretching timescale is set equal to that associated with viscous diffusion of vorticity. Hence the Reynolds number measures not only the strength of the convective forces relative to viscous forces, but also the relative magnitude of the vorticity-associated terms with respect to the strain terms: from (2.26)–(2.28) it follows that $\Gamma/\gamma = \pi Re$.

3. Numerical solution

A combination of finite-difference and spectral methods is used. Represent ω and ψ formally as

$$\omega(r,\theta,t) = \sum_{n=-\frac{1}{2}N}^{\frac{1}{2}N-1} \hat{\omega}_n(r,t)\,\mathrm{e}^{\mathrm{i}n\theta}, \tag{3.1}$$

$$\psi(r,\theta,t) = \sum_{n=-\frac{1}{2}N}^{\frac{1}{2}N-1} \hat{\psi}_n(r,t)\,\mathrm{e}^{\mathrm{i}n\theta}, \tag{3.2}$$

where $r\in[0,\infty)$ and $\theta\in[0,2\pi)$. The truncated Fourier series (3.1) and (3.2) are substituted into (2.10)–(2.13) to obtain evolution equations for the coefficients $\hat{\omega}_n$ and $\hat{\psi}_n$, $n=-\frac{1}{2}N,\ldots,\frac{1}{2}N-1$. There are two parts to the calculation: (i) solution of the Poisson equation; (ii) time advancement.

3.1. *Poisson equation*

Substituting (3.1) and (3.2) into (2.13) and invoking the (discrete) Fourier transform results in N ordinary (uncoupled) differential equations for the complex variables $\hat{\psi}_n(r)$, $n=-\frac{1}{2}N,\ldots,\frac{1}{2}N-1$:

$$\frac{\mathrm{d}^2\hat{\psi}_n}{\mathrm{d}r^2}+\frac{1}{r}\frac{\mathrm{d}\hat{\psi}_n}{\mathrm{d}r}-\frac{n^2}{r^2}\hat{\psi}_n = -\hat{\omega}_n, \quad n=-\tfrac{1}{2}N,\ldots,\tfrac{1}{2}N-1. \tag{3.3}$$

(i) $n=0$:

For the axisymmetric component of the vorticity field,

$$\frac{\mathrm{d}^2\hat{\psi}_0}{\mathrm{d}r^2}+\frac{1}{r}\frac{\mathrm{d}\hat{\psi}_0}{\mathrm{d}r} = -\hat{\omega}_0. \tag{3.4}$$

From (2.16) and (3.1) we obtain

$$\Gamma = \int \omega\,\mathrm{d}A = 2\pi\int_0^\infty \hat{\omega}_0(r)\,r\,\mathrm{d}r. \tag{3.5}$$

So when $\Gamma\neq 0$, it follows from (2.17) that

$$\hat{\psi}_0(r)\to\frac{\Gamma}{2\pi}\ln(r), \quad r\to\infty. \tag{3.6}$$

Since the velocity derived from ω and not ψ itself is required, we put $\hat{v}_{\theta_0} = -\partial\hat{\psi}_0/\partial r$ into (3.4), giving

$$\frac{\mathrm{d}\hat{v}_{\theta_0}}{\mathrm{d}r}+\frac{1}{r}\hat{v}_{\theta_0} = \hat{\omega}_0(r), \tag{3.7}$$

with boundary conditions, $\hat{v}_{\theta_0}(0)=0$, $\hat{v}_{\theta_0}(r\to\infty)=0$. The formal solution of (3.7) is

$$\hat{v}_{\theta_0}(r) = \frac{1}{r}\int_0^r u\hat{\omega}_0(u)\,\mathrm{d}u. \tag{3.8}$$

(ii) $n=1$:

The $n=1$ equation can be recast using the transformation $\hat{\psi}_1 = r\phi(r)$, giving

$$r\frac{\mathrm{d}^2\phi}{\mathrm{d}r^2}+3\frac{\mathrm{d}\phi}{\mathrm{d}r} = -\hat{\omega}_1(r). \tag{3.9}$$

From (2.17) and (3.6), $\phi(\infty) = 0$. Equation (3.9) was integrated from $r = 0$ with boundary conditions $\phi = 0, \mathrm{d}\phi/\mathrm{d}r = 0$. The solution was then corrected by subtracting off $\phi(\infty)$ to give the required boundary condition at infinity.

(iii) $n \geqslant 2$:

The boundary conditions are

$$\hat{\psi}_n(r = 0) = 0, \quad \hat{\psi}_n(r \to \infty) = 0, \tag{3.10}$$

for all $n \geqslant 2$. Thus (3.3) can be solved as a standard two-point boundary-value problem.

The radial equations were solved on a finite domain obtained by a coordinate mapping

$$r = R \tan(\pi\zeta), \tag{3.11}$$

which maps $r \in [0, \infty)$ onto $\zeta \in [0, \frac{1}{2})$, where R is a parameter. The stretched equations were solved numerically using fourth-order finite differences. The $n = 0$ and $n = 1$ equations can be integrated as ODE's while for $n \geqslant 2$ a pentadiagonal system results which can be solved directly in $O(N)$ operations. Overall, the Poisson solver requires $O(N^2)$ operations. When the $\hat{\psi}_n, n = -\frac{1}{2}N, \frac{1}{2}N-1, n \neq 0$ are known the non-axisymmetric velocity field is constructed from spectral θ-differentration and fourth-order finite-differenced ζ-differentration.

3.2. *Time advancement*

Substituting (3.1) into (2.10), using (2.11) and (2.12) and taking the Fourier transform we obtain

$$\begin{aligned}\frac{\partial\hat{\omega}_n}{\partial t} = \nu\left\{\frac{\partial^2\hat{\omega}_n}{\partial r^2} + \frac{1}{r}\frac{\partial\hat{\omega}_n}{\partial r} - \frac{n^2}{r^2}\hat{\omega}_n\right\} + \frac{\gamma}{2r}\frac{\partial}{\partial r}(r^2\hat{\omega}_n) \\ - \frac{1}{r}\mathscr{F}\left[\frac{\partial}{\partial r}(\omega r v_r)\right]_n - \frac{1}{r}\mathscr{F}\left[\frac{\partial}{\partial\theta}(\omega v_\theta)\right]_n \\ + \frac{1}{2r}(2\beta-\gamma)\left[\frac{\partial}{\partial r}(r^2\hat{\omega}_{n-2}) + \frac{\partial}{\partial r}(r^2\hat{\omega}_{n+2})\right] \\ + \tfrac{1}{2}(2\beta-\gamma)\left[(n+2)\hat{\omega}_{n+2} - (n-2)\hat{\omega}_{n-2}\right], \quad n = -\tfrac{1}{2}N, \ldots, \tfrac{1}{2}N-1,\end{aligned} \tag{3.12}$$

giving N equations, for the coefficients $\hat{\omega}_n(r)$. Coordinate stretching is employed here also, but details are omitted in the interests of clarity.

The boundary conditions for the equations (3.12) are

$$\hat{\omega}_n(r = \infty) = 0, \quad \text{all } n, \tag{3.13a}$$

$$\hat{\omega}_n(r = 0) = 0, \quad n \neq 0, \tag{3.13b}$$

$$\frac{\mathrm{d}\hat{\omega}_0}{\mathrm{d}r}(r = 0) = 0, \quad n = 0. \tag{3.13c}$$

The $\hat{\omega}_n$ were advanced in time using a second-order explicit predictor. These values were then updated in a Crank–Nicolson, semi-implicit, two-point corrector scheme. The nonlinear terms were evaluated as the right-hand side of the linear problem resulting from the Crank–Nicolson formulation. The discretized approximations to the linear terms using five-point differentiation rules form a pentadiagonal matrix and can be inverted directly. The scheme gives updated values for $\hat{\omega}_n(t+\delta t)$, $n = -\frac{1}{2}N, \ldots, \frac{1}{2}N-1$, where δt is the fixed time-step. At each implementation of the

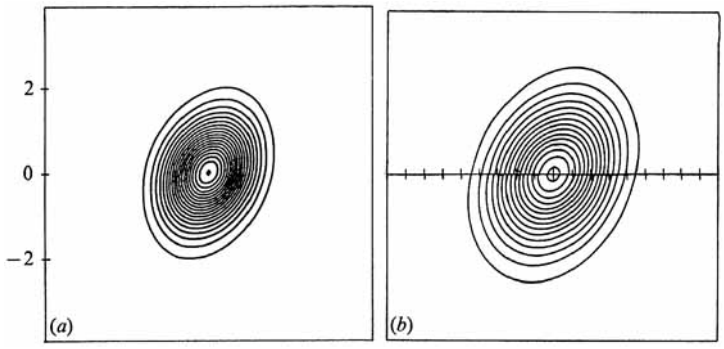

FIGURE 1. Equilibrium shape of a strained vortex in a non-axisymmetric strain field ($\gamma = 4$, $\beta = 3$). $Re = \Gamma/2\pi\nu = 10$. (*a*) present $|\omega_{\min}| = 1, |\Delta\omega| = 1$; (*b*) Robinson & Saffman (1984).

Crank–Nicolson scheme, the nonlinear terms in (3.12) were evaluated using velocity field information obtained from the Poisson solver with right-hand side given by the latest $\hat{\omega}_n(t+\delta t)$. This introduces iteration into the time advancement, in order to maintain stability with moderate δt (see also Peace & Riley 1983). Generally 3–4 iterations were required for convergence in the $\hat{\omega}_n(t+\delta t)$.

3.3. *Testing of code; non-axisymmetric strained vortex*

A strong test requires a non-axisymmetric strain field which introduces the coupled terms in the time-advancement equations. The test used was the equilibrium strained vortex in a non-axisymmetric strain field (Robinson & Saffman 1984). Strain-field parameters are assigned values $\gamma = 4$, $\beta = 3$ to correspond to Robinson & Saffman's $\epsilon = \frac{1}{2}$ which is a measure of the anisotropy. Since $\nu = 1$, the only free parameter is the Reynolds number

$$Re = \frac{\Gamma}{2\pi\nu} = \frac{\Gamma}{2\pi}. \tag{3.14}$$

The non-axisymmetric equilibrium states were found by placing symmetric vortices at the centre of the strain field and allowing them to relax. Equilibrium was assumed when the fractional change in the error diagnostic $\max_{n\neq 0}|\hat{\omega}_n(\zeta_j)|$ was less than 10^{-3} over several time-steps. A comparison with a result of Robinson & Saffman ($Re = 10$) is given in figure 1. By scaling the value of the maximum vorticity over the maximum for the same vortex in an axisymmetric strain field, a quantitative comparison can also be made (table 1). The agreement is good.

In figure 2, for a fixed strain-field strength and geometry ($\epsilon = \frac{1}{2}$ in the notation of Robinson & Saffman), Re is varied from 0.1 to 160. Each frame shows the equilibrium state reached from the axisymmetric Burgers vortex initial condition. Since the viscosity and strain intensification are fixed for this series of flows, the Reynolds number can also be taken as a measure of the strength of inertial effects relative to those induced by the strain field and viscous diffusion.

At very low Reynolds numbers ($Re = 0.1, 1$) the strain field dominates and the vortex is most distorted. The axis of elongation almost corresponds to the $\theta = \frac{1}{2}\pi$ direction, where the (x, y)-plane strain is a minimum, demonstrating that the vortex self-induction is only weakly active. As the Reynolds number increases ($Re = 5, 10$), the axis of elongation slowly rotates and in each case assumes an orientation that appears to represent a balance between strain and vortex induction. Eventually the vortex becomes so strong that the directional effects of the strain are overcome.

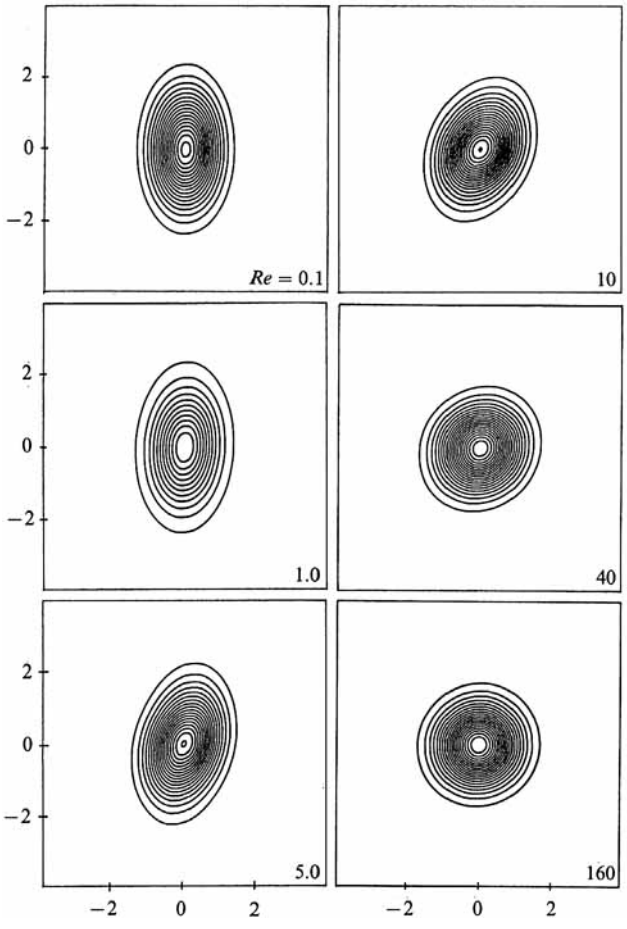

FIGURE 2. Equilibrium state of strained vortices in a non-axisymmetric strain field ($\gamma = 4, \beta = 3$). Minimum contour $|\omega_{\min}| = Re/10$, intervals between contours are $|\Delta\omega| = Re/10$.

Re	ω_M/ω_M(BV)	ω_{Max} R & S
0	—	0.87
0.1	0.870	—
1	0.872	—
5	0.905	—
10	0.953	0.95
40	0.996	—
100	0.999	1.00
160	1.000	—

TABLE 1. Comparison between the maximum value of the equilibrium vorticity in a non-axisymmetric (ω_M) and axisymmetric (ω_M(BV)) strain field obtained here and by Robinson & Saffman (1984) (ω_{Max} R & S).

Vortex deformation is not evident on the scale of these plots. The resulting equilibrium resembles the result for a Burgers vortex in an axisymmetric strain field of strength γ (see also table 1). This conclusion is consistent with the results of Lin & Corcos (1984) and Neu (1984*b*).

4. Merging of strained vortices

The merging of an isolated pair of equal Burgers vortices was studied in considerable detail. Most events were considered in an axisymmetric strain field; however, one case was run in which the strain field was non-axisymmetric. A list of the cases studied is given in table 2.

4.1. *Time-steps*

The approximate time-step chosen was, $\delta t \approx 1/(\mathrm{N\,Re})$, where N is the number of grid points in both the ζ- and θ-directions. Larger time-steps could be used if the number of iterations performed per time-step was increased. The optimum compromise involved four iterations with each step. Attempts to improve the code took two paths: (i) Dealiasing was performed on the nonlinear convolution terms of the time-marching equation to try to improve the stability of the solution method. It was believed that if aliasing errors were present, they may have restricted the size of the time-step that could be used. Dealiasing had no effect on the solution stability and was not used subsequently as it required significantly more computation than the aliased version. (ii) Symmetries present in the merging events were used to reduce by half the number of independent Fourier coefficents.

For all merging events, the r–ζ stretching parameter, (3.11), was fixed at $R = 1.2$.

4.2. *Initial conditions*

Initial conditions were adopted of the form,

$$\omega(x, y, 0) = \frac{-\Gamma}{2\pi}\{\mathrm{e}^{-(x-x_0)^2-y^2} + \mathrm{e}^{-(x+x_0)^2-y^2}\}, \tag{4.1}$$

where $\Gamma = 2\pi Re$. This is a superposition of two axisymmetric vorticity distributions each with circulation $\frac{1}{2}\Gamma$. If either distribution was centred at the origin it would correspond to an equilibrium solution. For most calculations, $x_0 = 2$ was used, since it was apparent that the later stages of merging were not strongly dependent on x_0, provided $x_0 > 1$ (see figure 5). It is expected that the flow with initial conditions (4.1) will asymptotically relax towards an axisymmetric Burgers vortex with circulation Γ.

4.3. *Results of the merging events*

Figures 3–7 show 'snapshots' of vorticity contours at sequential times during merging events for $Re = \Gamma/2\pi\nu = 40$ to 1280. At all Reynolds numbers the merging events show similar qualitative features. Initially all vortex pairs rotate about each other with an angular velocity which can be approximated using a point-vortex model. As the vortices rotate, their cores (or regions of maximum vorticity) spiral inwards, eventually merging into a single region of strong vorticity. During their approach, the cores rotate increasingly more rapidly, forming a region of differential rotation. On the leading edge of the vortex, the vorticity gradient itensifies. This band of high-gradient vorticity is stretched azimuthally by the vortex cores as they spiral inwards. Viscosity acts locally to diffuse the vorticity gradients on much shorter timescales than the global process of relaxation to a single axisymmetric Burgers vortex.

Re	β	t_f	Grid
0.1	2	1.2	32^2
1	2	1.2	32^2
5	2	1.2	32^2
10	2	1.2	32^2
20	2	1.2	32^2
40	2	1.0	64^2
80	2	1.0	64^2
160	2	0.95	128^2
160	4	0.8	128^2
320	2	0.9	128^2
640	2	0.14	128^2
1280	2	0.105	256^2

TABLE 2. Parameters used for merging of two equal Burgers vortices, t_f = simulation time, $Re = \Gamma/2\pi\nu, \gamma = 4$.

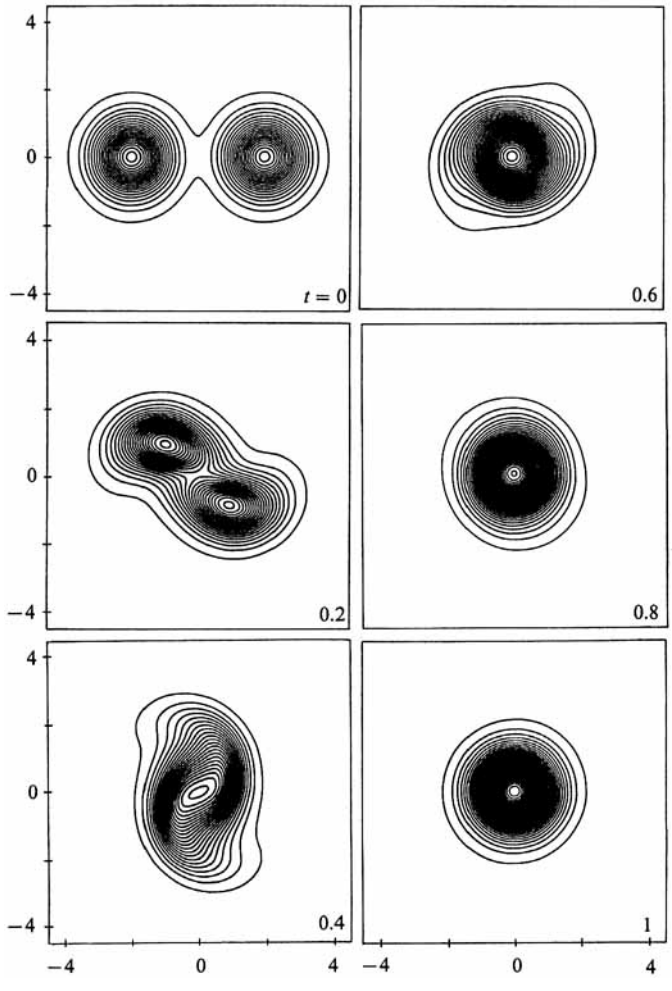

FIGURE 3. Merging of two like-signed vortices in an axisymmetric strain field ($Re = \Gamma/2\pi\nu = 40$). The minimum contour is $|\omega_{min}| = 1.0$ and all contour intervals are $|\Delta\omega| = 2.0$.

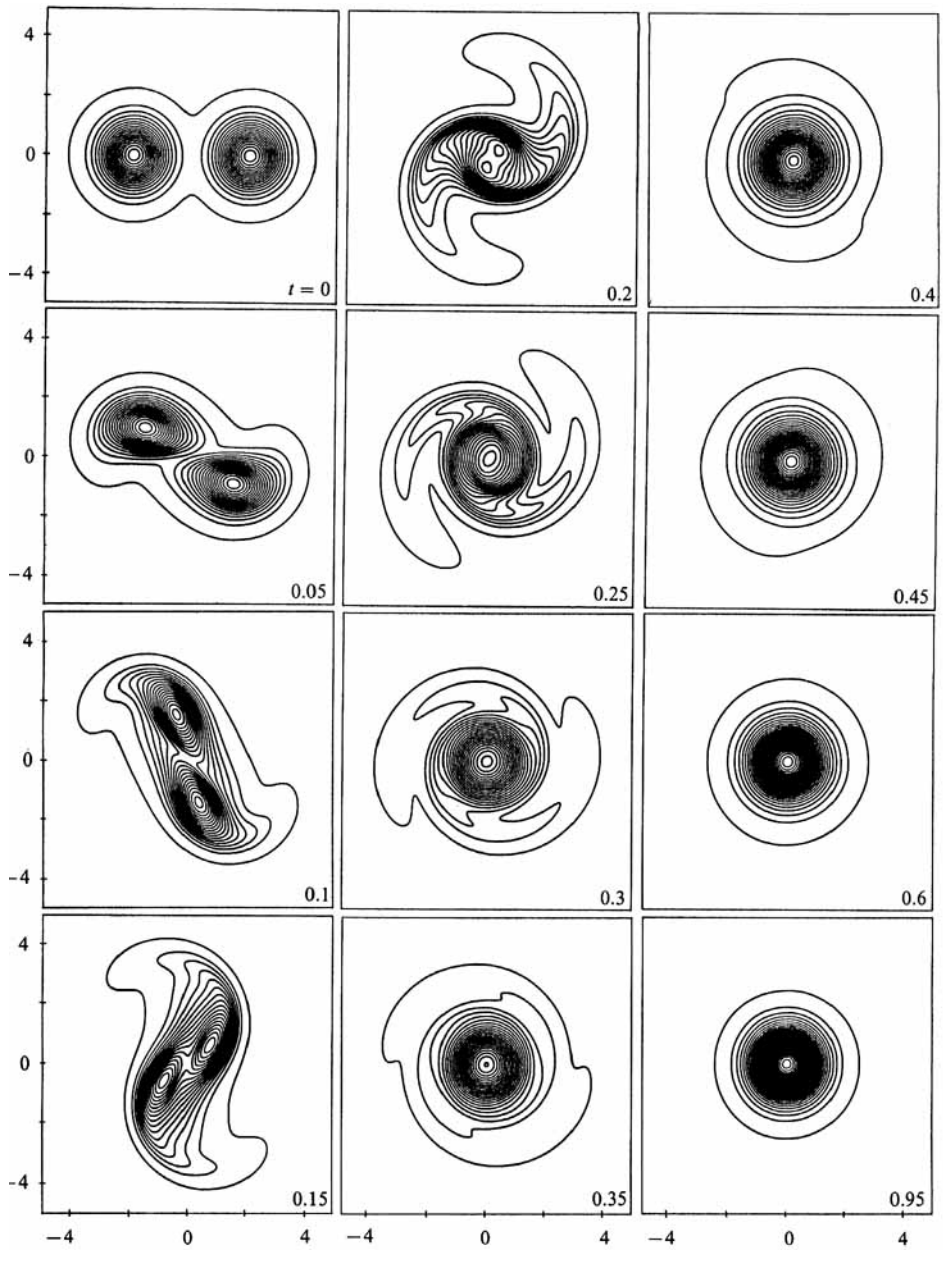

FIGURE 4. Merging of two like-signed vortices in an axisymmetric strain field ($Re = \Gamma/2\pi\nu = 160$). The minimum contour is $|\omega_{\min}| = 1.0$ and all contour intervals are $|\Delta\omega| = 9.0$.

Consider the following dimensionless timescales over which the global processes act:

$$t_\Gamma = \frac{4\pi^2 d^2}{\Gamma} = \frac{2\pi d^2}{Re}, \tag{4.2}$$

$$t_\gamma = 4\gamma^{-1} = 1, \tag{4.3}$$

$$t_\nu = \frac{a^2}{\nu} = 1, \tag{4.4}$$

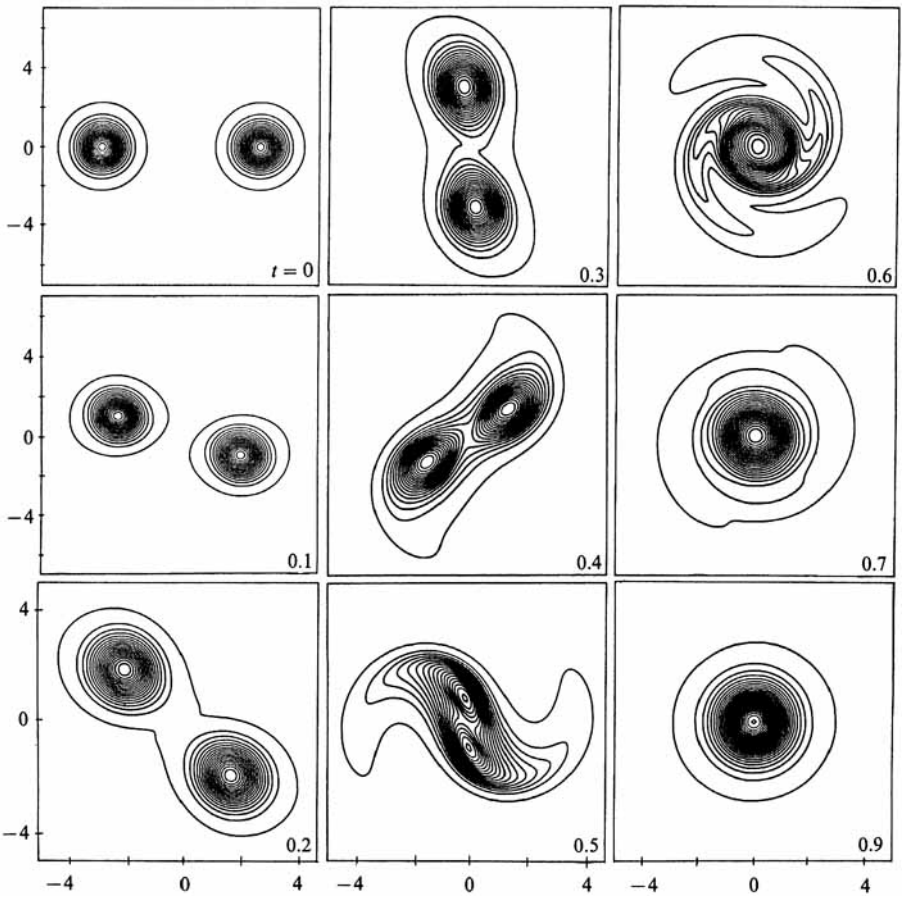

FIGURE 5. Merging of two like-signed vortices in an axisymmetric strain field ($Re = \Gamma/2\pi\nu = 160$). The minimum contour is $|\omega_{\min}| = 1.0$ and all contour intervals are $|\Delta\omega| = 9.0$. Initial separation $d = 8$.

where the t_Γ, t_γ and t_ν are the convective, straining and viscous timescales respectively, the latter associated with a vortex of radius a (see 2.20). The timescales t_ν and t_γ are fixed and only t_Γ varies (inversely) with the Reynolds number. At $Re = 10, 40$ the convection timescale $t_\Gamma > 1$, indicating that merging is controlled largely by viscosity and the strain field. The $Re = 10$ case in particular, shows viscous and strain effects moving the vorticity distribution towards the equilibrium solution, while experiencing relatively little interaction with the weak vorticity. The merging depicted in figure 3 at $Re = 40$, is qualitatively similar to the subharmonic vortex pairing event calculated by Lin & Corcos (1984) (their figure 20) following primary instability of a Burgers vortex layer.

With increasing Reynolds number the vorticity changes its behaviour from an essentially passive scalar to play an active role in the dynamics of the evolution. When the Reynolds number $Re = 160$, (figure 4) $t_\Gamma < t_\gamma, t_\nu$ and vorticity-related effects start to become appreciable. Regions of weaker vorticity are left behind the faster rotating and stronger cores, forming embryonic spiral arms. Vorticity contours in front of the cores bunch up, highlighting regions of higher vorticity gradient. These are stretched along the paths of the cores but are quickly diffused since here viscous effects are comparable with those associated with the vorticity. Enhancement

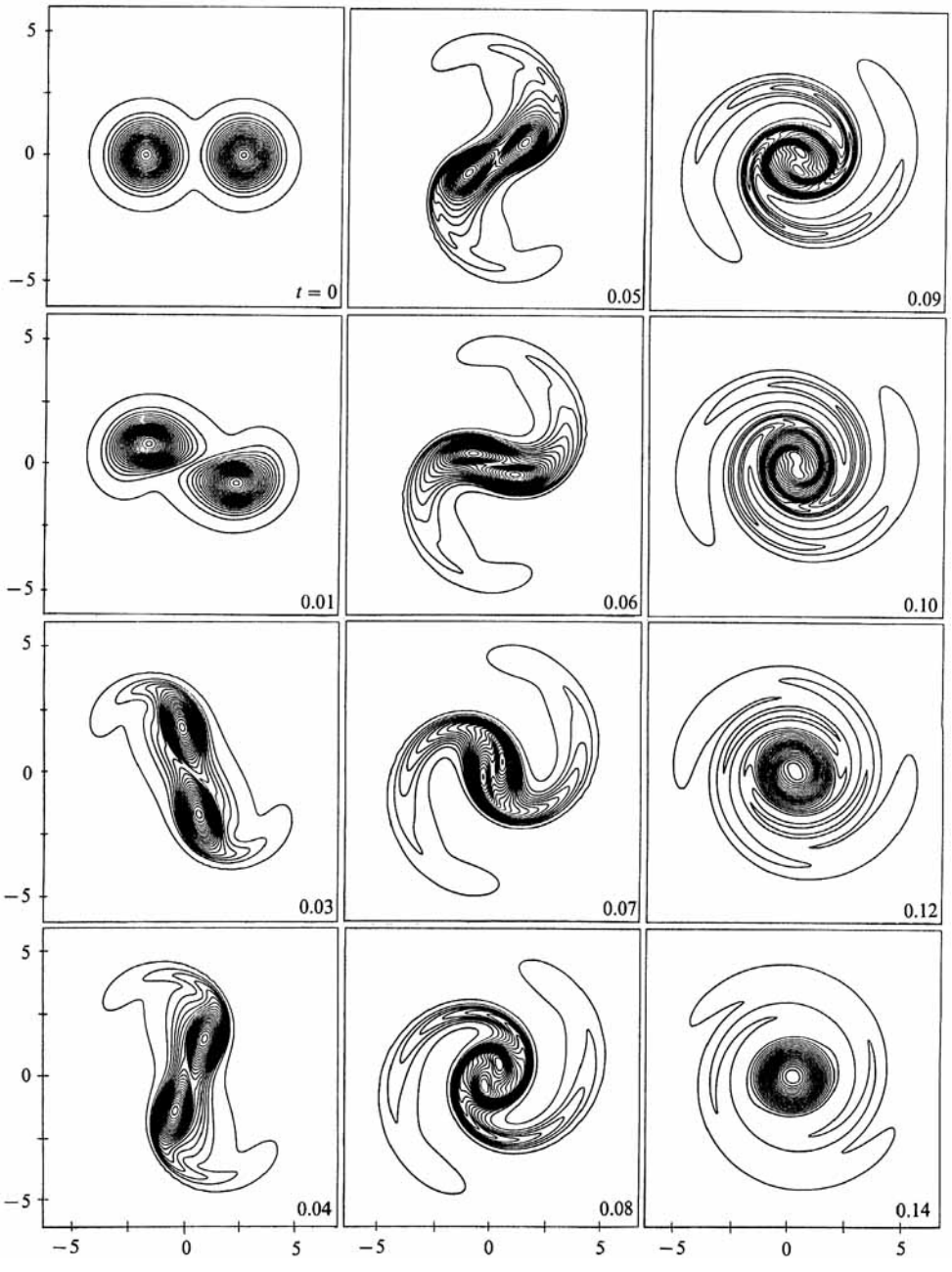

FIGURE 6. Merging of two like-signed vortices in an axisymmetric strain field ($Re = \Gamma/2\pi\nu = 640$). The minimum contour is $|\omega_{\min}| = 3.0$ and all contour intervals are $|\Delta\omega| = 30.0$.

of vorticity gradients helps viscosity to (locally) dominate the action of convection. The short arms also quickly diffuse to form a single vortex of convex form. Contour densities increase between $t = 0.6$ and $t = 0.95$ in figure 4 indicating that the strain-field vortex intensification is not complete even though the vortex is circular. For the highest two Reynolds-number cases shown, $Re = 640$ (figure 6) and $Re = 1280$ (figure 7), $t_\Gamma \ll t_\gamma, t_\nu$ and the convective processes dominate the flow evolution. The same

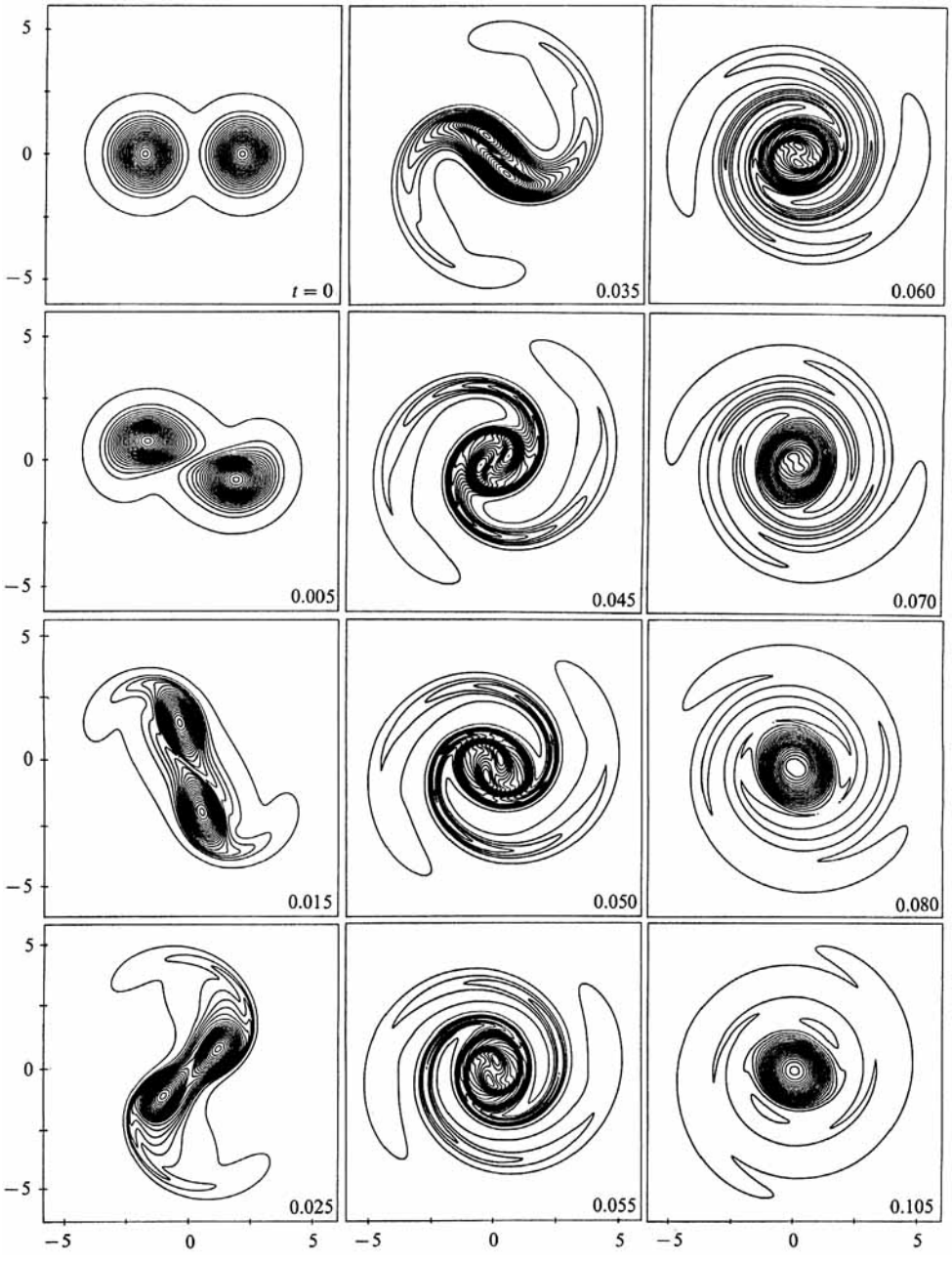

FIGURE 7. Merging of two like-signed vortices in an axisymmetric strain field ($Re = \Gamma/2\pi\nu = 1280$). The minimum contour is $|\omega_{\min}| = 3.0$ and all contour intervals are $|\Delta\omega| = 60.0$.

features described in the $Re = 160$ cases are present but are more highly developed. The strong gradient regions lengthen into thinner spiral bands before diffusing, as do the vortex arms. One effect which is not clear in the $Re = 160$ case is thinning of the spiral arms at their 'shoulders'. Since the arms are being thrown off much more rapidly than the vorticity can diffuse, the vorticity in the arms should be nearly conserved, thus as the arms extend they become thinner at the shoulder as this is

where the extension occurs. It is interesting to note that in the later stages of the axisymmetrization, the arms appear to separate to some extent from the core of the vortex. For the flows of figures 6 and 7, fractional changes in Γ, calculated as the area integral of ω, remained constant to $O(10^{-5})$ over computed times.

Figures 8 and 9 show vorticity plotted on radial cuts in the (r, θ)-plane at $\theta = 0$ (the positive x-axis) and $\theta = \frac{1}{2}\pi$ (the positive y-axis). At $Re = 10$ (not shown) the vorticity convects and diffuses to the final Burgers vortex form. The $Re = 160$ case (figure 8) illustrates a region of high vorticity gradient within the vortex core in the x-axis plot at $t = 0.2$. Near convergence to the Burgers vortex form occurred in all three cases $Re = 10, 40, 160$ within computed time.

The finer arm structure in the $Re = 1280$ case (figure 9) can be seen at $t = 0.06$, where two oscillations can be seen in the x-axis plot. Earlier times in this merging event show the movement of the separate vortex cores towards each other to form a single, larger core. Although the vortex is all but axisymmetric (compare the x- and y-axis plots and see the final frames of figure 7) at the final time computed for this event ($t = 0.105$), the strain field clearly requires more time to intensify the vorticity into its final equilibrium form.

The highest-Reynolds-number merging events examined in this discussion qualitatively resemble the strictly two-dimensional vortex merging considered by Melander *et al.* (1987) and Melander, Zabusky & McWilliams (1988). They considered the merging of two vortices with compact support in a two-dimensional box with periodic boundary conditions. A spectral method was employed to solve the problem where no strain field was present. To simulate very high-Reynolds-number flows, they employed a hyperviscosity term in their governing equations. This allowed them to study mechanisms believed to be present in the inviscid limit of flows described by the Navier–Stokes equations. In an inviscid fluid for two vortices not subject to a strain field, merging does not necessarily follow. Melander *et al.* give a maximum intercentroid distance of

$$d = 3.4(A/\pi)^{\frac{1}{2}}, \tag{4.5}$$

where A is the vortex area, for two identical, piecewise-constant circular vortices if merging is to occur.

For the problem currently being investigated, viscosity and strain-field strength are constant and linked through the scaling adopted (§2.4). These two quantities are finite and hence merging is guaranteed eventually, albeit on a timescale that may be large compared with t_Γ if the intercentroid distance is initially large. This is also true, therefore, for the equivalent two-dimensional flow without a strain field, as defined in §2.3. Increasing the Reynolds number increases the vorticity relative to the two fixed effects. An inviscid limit to this event can be found equivalently by fixing the geometry for the initial condition and the strength of the vortices (each vortex is distributed as $\frac{1}{2}\Gamma^* \mathrm{e}^{-r^2}$ about the points $(-2, 0), (2, 0)$, where Γ^* is some normalized value for the circulation) and sending both ν and γ to zero.

This limit was considered using Jacobs' (1987) contour-dynamics code which employed eight nested constant-vorticity regions. The results at two equivalent times are shown in figure 10. The good qualitative agreement in the first comparison between the two simulations suggest that the $Re = 1280$ case gives a good approximation to the inviscid limit for early times. As the vortices continue to merge, however, the cores in the viscous case rotate more rapidly (cf. $t\Gamma/d^2 = 25$), suggesting that some intensification has occurred by this stage.

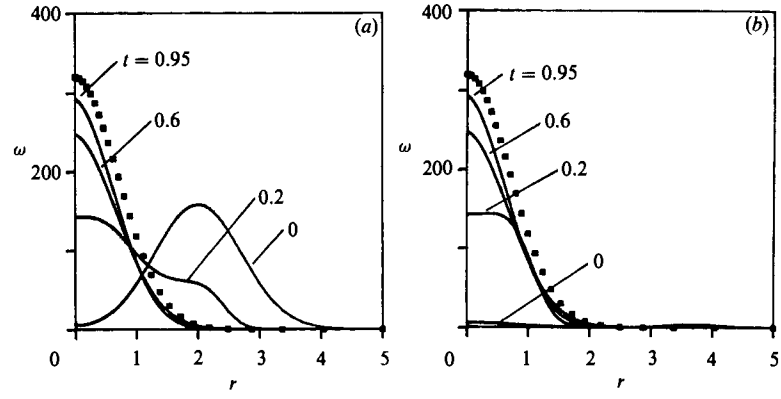

FIGURE 8. Distribution of vorticity along radial cuts in the computational plane for the $Re = \Gamma/2\pi\nu = 160$ merging event. The directions of the two radial lines are (*a*) $\theta = 0$, (positive-x axis), (*b*) $\theta = \frac{1}{2}\pi$, (positive-y axis). ■ indicates asymptotic Burgers vortex.

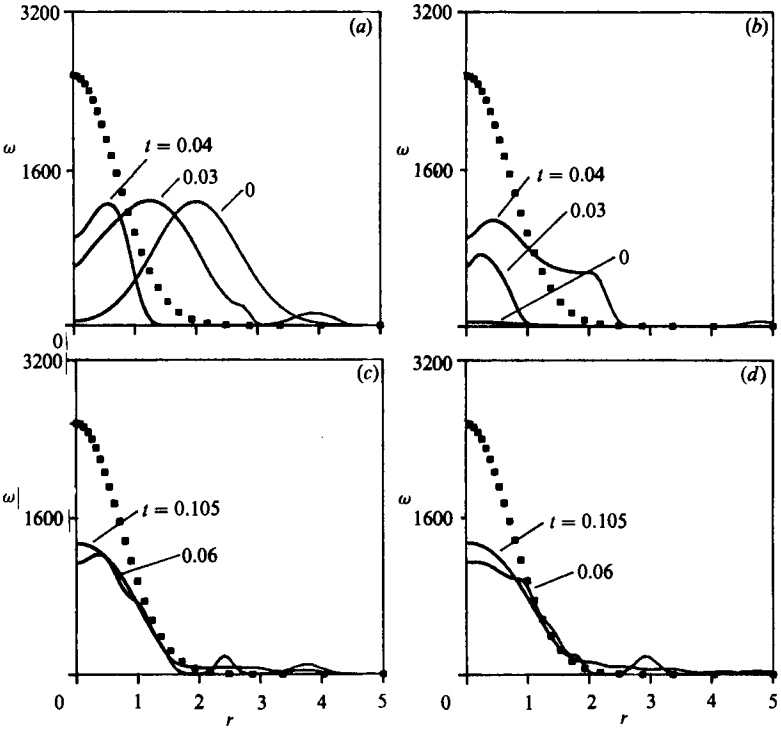

FIGURE 9. Distribution of vorticity along radial cuts in the computational plane for the $Re = \Gamma/2\pi\nu = 1280$ merging event. The directions of the radial lines are (*a*, *c*) $\theta = 0$, (positive-x axis); (*b*, *d*) $\theta = \frac{1}{2}\pi$, (positive-y axis). ■ indicates asymptotic Burgers vortex.

4.4. *Energy spectra for homogeneous turbulence*

The results obtained in the merging events are used to calculate an energy spectrum for a model of isotropic turbulence in incompressible flow. Lundgren (1982) assumes that homogeneous turbulence within a box of dimension $\bar{L}$ can be modelled using a collection of randomly distributed vortex tubes, each tube consisting of a relaxing

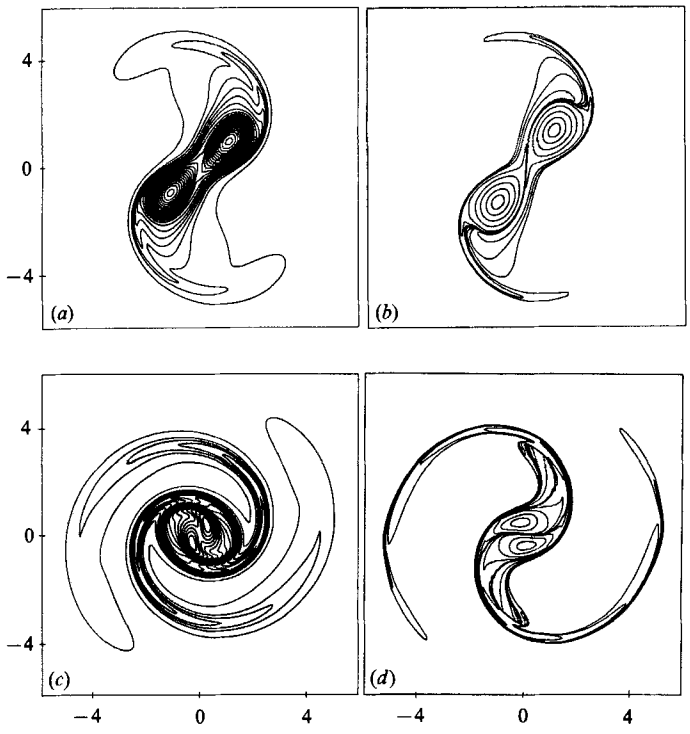

FIGURE 10. Comparison between the contour-dynamics code of Jacobs (1987) (b, d) and the present solution method (a, c). (a) $\Gamma/(2\pi\nu) = 1280$, $\bar{t}\Gamma/d^2 = 12.5$; (b) $\gamma = \nu = 0$, $\bar{t}\Gamma/d^2 = 12.5$; (c) $\Gamma/2\pi\nu = 1280$, $\bar{t}\Gamma/d^2 = 25$; (d) $\gamma = \nu = 0$, $\bar{t}\Gamma/d^2 = 25$.

vortex spiral resulting perhaps from the roll-up of a vortex sheet or the merging of two vortices. Returning to dimensional coordinates, let $\bar{\omega}(\bar{r}, \bar{t})$ be the vorticity distribution for a typical vortex tube: this may be a relaxing spiral or, as now, a representative merging event. Using the result that, for homogeneous turbulence, the instantaneous energy spectrum $\bar{E}(\bar{k}, \bar{t})$ can be related to the power spectrum of the vorticity distribution $\bar{E}_{\omega\omega}(\bar{k}, \bar{t})$ as

$$\bar{E}(\bar{k}, \bar{t}) = \bar{E}_{\omega\omega}(\bar{k}, \bar{t})/(2\bar{k}^2), \tag{4.6}$$

and replacing the ensemble average by a time integration (for statistically steady turbulence), Lundgren shows that $\bar{E}(\bar{k}, \bar{t})$ may be written as

$$\bar{E}(\bar{k}) = \frac{\bar{l}_0 \pi N_c}{\bar{k}\bar{L}^3} \int_0^{\bar{t}_c} S(\bar{t}) \left(I_0^2(\bar{k}, \bar{t}) + 2 \sum_{n=1}^{\infty} |I_n(\bar{k}, \bar{t})|^2 \right) \mathrm{d}\bar{t}, \tag{4.7}$$

$$I_n(\bar{k}, \bar{t}) = \int_0^{\infty} J_n(\bar{k}\bar{r})\, \bar{\omega}_n(\bar{r}, \bar{t})\, \bar{r}\, \mathrm{d}\bar{r}. \tag{4.8}$$

In (4.6)–(4.8), J_n is a Bessel function of the first kind, order-n, $\bar{\omega}_n$ is the nth coefficient in a Fourier series expansion for $\bar{\omega}(r, \theta, t)$,

$$S(\bar{t}) = \exp\left(\int_0^{\bar{t}} \bar{\gamma}(u)\, \mathrm{d}u \right) = \mathrm{e}^{A(\bar{t})} = \mathrm{e}^{\bar{\gamma}\bar{t}}, \tag{4.9}$$

$\bar{l}_0$ is the assumed length of the vortex tube at the start of the event ($\bar{l}(\bar{t}) = \bar{l}_0 S(\bar{t})$), N_c is the rate at which new vortex tubes are being created within the box (assumed

constant), $\bar{k}$ is the wavenumber and $\bar{t}_c$ is the duration of the vortex event. The choice of $\bar{t}_c$ is somewhat arbitrary and will be discussed later. Equation (4.7) can be rewritten as

$$\bar{E}(\bar{k}) = \frac{\bar{l}_0 \pi N_c}{\bar{k}\bar{L}^3} \bar{P}(\bar{k}), \tag{4.10}$$

where

$$\bar{P}(\bar{k}) = \int_0^{\bar{t}_c} S(\bar{t}) \left(I_0^2(\bar{k}, \bar{t}) + 2 \sum_{n=1}^{\infty} |I_n(\bar{k}, \bar{t})|^2 \right) \mathrm{d}\bar{t}. \tag{4.11}$$

The energy dissipation can also be calculated similarly as

$$\bar{\epsilon} = 2\pi\bar{\nu} \frac{\bar{l}_0 N_c}{\bar{L}^3} \bar{M}, \tag{4.12}$$

where

$$\bar{M} = \int_0^{\bar{t}_c} S(\bar{t}) \int_0^{\infty} \left(\bar{\omega}_0^2 + 2 \sum_{n=1}^{\infty} |\bar{\omega}_n|^2 \right) \bar{r}\, \mathrm{d}\bar{r}\, \mathrm{d}\bar{t}. \tag{4.13}$$

Combining (4.10) and (4.12) then gives

$$\bar{E}(\bar{k}) = \frac{\bar{\epsilon}}{2\bar{k}\bar{\nu}} \frac{\bar{P}(\bar{k})}{\bar{M}}. \tag{4.14}$$

It is usual to normalize $\bar{k}$ using a wavenumber representative of the dissipation range. Following Hinze (1975), we take

$$\bar{k}_d = \frac{1}{\bar{\eta}} = \left(\frac{\bar{\nu}^3}{\bar{\epsilon}} \right)^{-\frac{1}{4}}, \tag{4.15}$$

where $\bar{\eta}$ is the Kolmogorov microscale. The energy dissipation $\bar{\epsilon}$ can be estimated by approximating Townsend's (1951) assumption that the axial strain rate is proportional to the root-mean-square strain rate, and identifying this latter quantity with $\bar{\gamma}$ in the present merging Burgers vortex model. Hence,

$$\bar{\gamma} \approx \frac{1}{4} \left[\frac{\bar{\epsilon}}{\bar{\nu}} \right]^{\frac{1}{2}} \tag{4.16}$$

(Townsend takes $\bar{\gamma} = [\bar{\epsilon}/(15\bar{\nu})]^{\frac{1}{2}}$: the present approximation is slightly different for computational convenience); thus,

$$k_d = 4 \left(\frac{\bar{\gamma}}{4\bar{\nu}} \right)^{\frac{1}{2}}. \tag{4.17}$$

Putting $K = \bar{k}/\bar{k}_d$, and employing the scaling of §2.4, equation (4.14) can be written as

$$\bar{E}(K) = \frac{\bar{\epsilon}\bar{\nu}^{\frac{1}{2}}}{\bar{\gamma}^{\frac{3}{2}}} \frac{P(K)}{MK}, \tag{4.18}$$

where P and M are the dimensionless quantities resulting from $\bar{P}$ and $\bar{M}$ respectively, or using (4.16)

$$\frac{\bar{E}(K)}{(\bar{\epsilon}\bar{\nu}^5)^{\frac{1}{4}}} = 8 \frac{P(K)}{MK}. \tag{4.19}$$

If the vorticity distribution is a single Burgers vortex, then its spectrum is

$$\frac{\bar{E}(K)}{(\bar{\epsilon}\bar{\nu}^5)^{\frac{1}{4}}} = \frac{8}{K} \mathrm{e}^{-8K^2}. \tag{4.20}$$

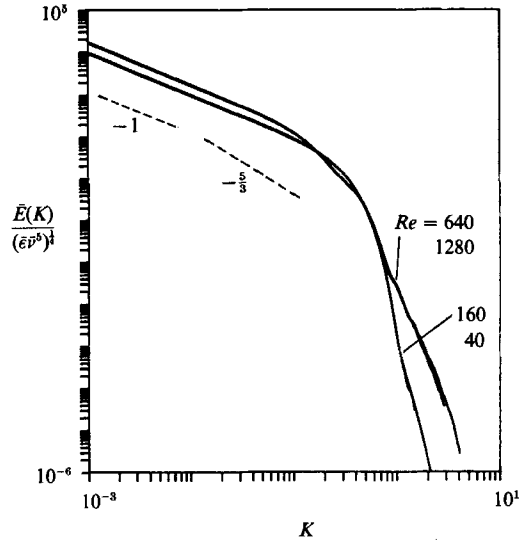

FIGURE 11. Energy spectra obtained from merging events, $Re = \Gamma/2\pi\nu = 40, 160, 640, 1280$.

For a vortex merging event $\bar{E}(K, t_c)$ was obtained by evaluating the integrals (4.11) and (4.13) using a time-step coarser than that employed in the numerical simulation. We note that t_c is a free parameter. When $t_c \to \infty$ the integrals for P and M go like $\exp(4t_c)$ and the spectrum is asymptotic to (4.20). We have taken $t_c \approx t_\Gamma$ for each Re (see (4.2)) on the assumption that at large Re the fine scales are generated inertially and have lifetimes of order t_Γ at most. Figure 11 shows the calculated spectra for four values of Re and figure 12 shows spectra calculated by omitting the axisymmetric term in (4.11). At small K the differences in $\bar{E}$ for $Re = 40, 160$ and $Re = 640, 1280$ can be attributed to $t_c \approx t_\gamma$ for the lower Re-values: the merging event has nearly reached its equilibrium form of figures 3 and 4.

At lower Reynolds number ($Re = 40, 160$) the dissipative range and the low-K range, where $\bar{E}$ goes like K^{-1}, are adjacent. However, for the high-Reynolds-number cases ($Re = 640, 1280$) a flattened portion of the spectrum is forming between the K^{-1} and the dissipative regions. This region has not been properly resolved owing possibly to uncertainties in fixing t_c and also to insufficiently high Re. The slope is not $-\frac{5}{3}$ as found by Lundgren, but then the vortex structure of the merging event is different from that of the Kaden Spiral: the latter contributes to the inertial range through many closely spaced and rolled up turns in a spiral band, while figure 7 shows only a few turns. Our maximum Re may be too low.

For comparison, figure 13 shows the well-known Heisenberg and Pao forms of the energy spectrum, which are respectively

$$\frac{\bar{E}(K)}{(\bar{\epsilon}\bar{\nu}^5)^{\frac{1}{4}}} = AK^{-\frac{5}{3}}\left(1+\frac{8}{3\alpha^2}K^4\right)^{-\frac{4}{3}}, \tag{4.21}$$

$$\frac{\bar{E}(K)}{(\bar{\epsilon}\bar{\nu}^5)^{\frac{1}{4}}} = AK^{-\frac{5}{3}}\exp\left(-\tfrac{3}{2}AK^{\frac{4}{3}}\right), \tag{4.22}$$

where the Kolmogorov constant A and the value of the dimensionless constant α in (4.21) have been taken as typical experimental values $A = 1.70, \alpha = 0.4$ (Hinze 1975, Chapter 3). In the dissipation range our calculations slightly favour Heisenberg's K^{-7}

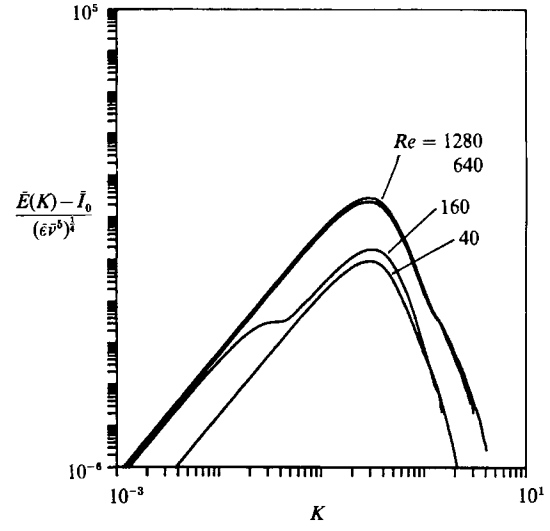

FIGURE 12. Energy spectra from merging events without the axisymmetric component (I_0). $Re = \Gamma/2\pi\nu = 40, 160, 640, 1280$.

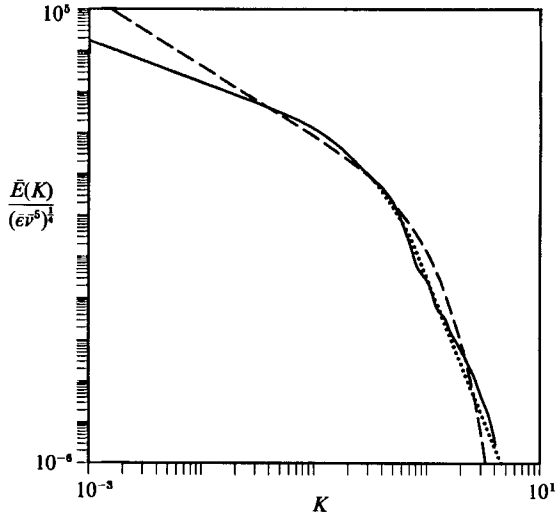

FIGURE 13. Energy spectra derived from merging events at Reynolds number $Re = \Gamma/2\pi\nu = 1280$ compared with models of Heisenberg (· · · · · ·) and Pao (– – – –).

form. The Heisenberg model was obtained assuming statistical independence of scales corresponding to large and small K, and this has been criticized in the literature. It is noted that the present result requires no such assumption since it is derived from a model based on a solution of the Navier–Stokes equations.

5. Cancellation of strained vortices

The cancellation of a pair of Burgers vortices of opposite sign is now discussed. Although the cancellation event produces less fine detail than the merging, simulation times required to produce near complete cancellation were longer. For

	β			
Re	2	4	8	16
0.1	×	×		
1	×	×		
5	×	×		
10	×	×		
20		×		
40	×		×	
80	×	×	×	
160	×	×	×	×

TABLE 3. Runs conducted for cancellation events in a strain field ($\gamma = 4$), $Re = \Gamma_0/2\pi\nu$.

this reason, the maximum Reynolds number that could reasonably be achieved was $Re = 160$. All calculations were performed on a 128^2 grid. Table 3 summarizes the cases considered.

5.1. *Moving reference frame*

The self-convection of two opposite-signed vortices causes them to move away from their initial positions to regions of the grid where points are less dense. To overcome this problem, the reference frame in which the grid is fixed was moved with the vortices with the consequence that the strain-field centre effectively moved with respect to the coordinate origin. The coordinate frame moves with a non-constant velocity which is arbitrarily chosen as the instantaneous y-component of the vorticity generated velocity $v_c(t)$, at the vortex centre, defined using

$$\boldsymbol{r}_{\text{mean}} = \frac{\int_A \boldsymbol{r}\,\omega\,\mathrm{d}A}{\int_A \omega\,\mathrm{d}A}, \tag{5.1}$$

where A denotes the half-plane $x < 0$. For the moving reference frame in Cartesian coordinates, the strain field is

$$\boldsymbol{u}_s = -\beta(t)\,x\boldsymbol{i} + [\beta(t) - \gamma(t)]\,(y - y_c(t))\,\boldsymbol{j} + \gamma(t)\,z\boldsymbol{k}, \tag{5.2}$$

where y_c is the y-displacement of the moving reference frame with respect to the frame of reference in which the velocity field at $r \to \infty$ has no spatially uniform component. The equation for y_c is then, from (2.3),

$$\frac{\mathrm{d}y_c}{\mathrm{d}t} = v_c(t) + (\beta - \gamma)\,y_c, \tag{5.3}$$

the solution of which is, with $y_c(0) = 0$,

$$y_c(t) = \mathrm{e}^{-(\gamma-\beta)t} \int_0^t \mathrm{e}^{(\gamma-\beta)t'} v_c(t')\,\mathrm{d}t'. \tag{5.4}$$

5.2. *Initial conditions*

The initial vorticity distributions were of the form

$$\omega(x, y, 0) = \frac{\Gamma_0}{\pi}\{\mathrm{e}^{-(x+x_0)^2-y^2} - \mathrm{e}^{-(x-x_0)^2-y^2}\}, \tag{5.5}$$

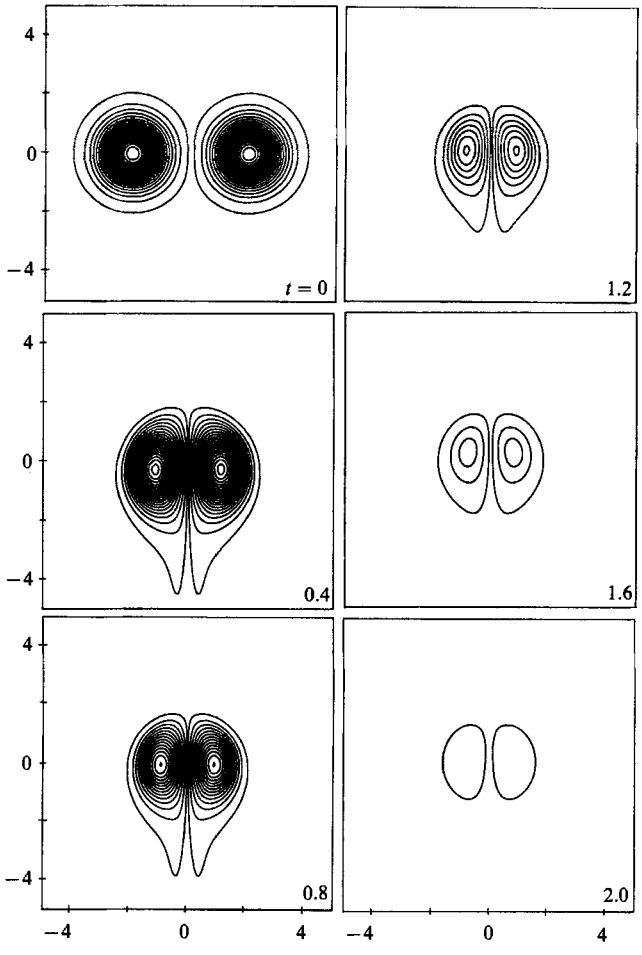

FIGURE 14. Cancellation of two opposite-signed vortices in an axisymmetric strain field, $\gamma = 4$, $\beta = 2$, $Re = \Gamma_0/2\pi\nu = 160$. The minimum contour is $|\omega_{\min}| = 5$ and all contour intervals are $|\Delta\omega| = 15$.

where Γ_0 is now the circulation of each concentration of vorticity so that the Reynolds number here is based on the initial circulation of one vortex ($Re = \Gamma_0/2\pi\nu$). The separation was again chosen to be $x_0 = 2$. Symmetry about $x = 0$ was not assumed.

5.3. *Results of cancellation*

At low to moderate Re vorticity acts as a passive scalar, cancelling as the vortex centres are forced together by the strain. An example of merging in an axisymmetric strain field ($\beta = 2$) is shown in figure 14 at $Re = 160$. As Re is increased for the same strength of strain field, vorticity begins to play a more active role in the event. At $Re = 160$, $\beta = 4$ (figure 15) the vorticity is the more dominant feature, significant translation is undergone by the pair and large tails form. For the same $Re = 160$, but with $\gamma = 4$, $\beta = 16$ the strong strain in the x-direction forces the two vortices together. They become extremely elongated (figure 16) and cancellation occurs very rapidly.

To study the cancellation event in more detail, a number of quantitative diagnostics were computed during the evolution. Examples can be seen in figures 17

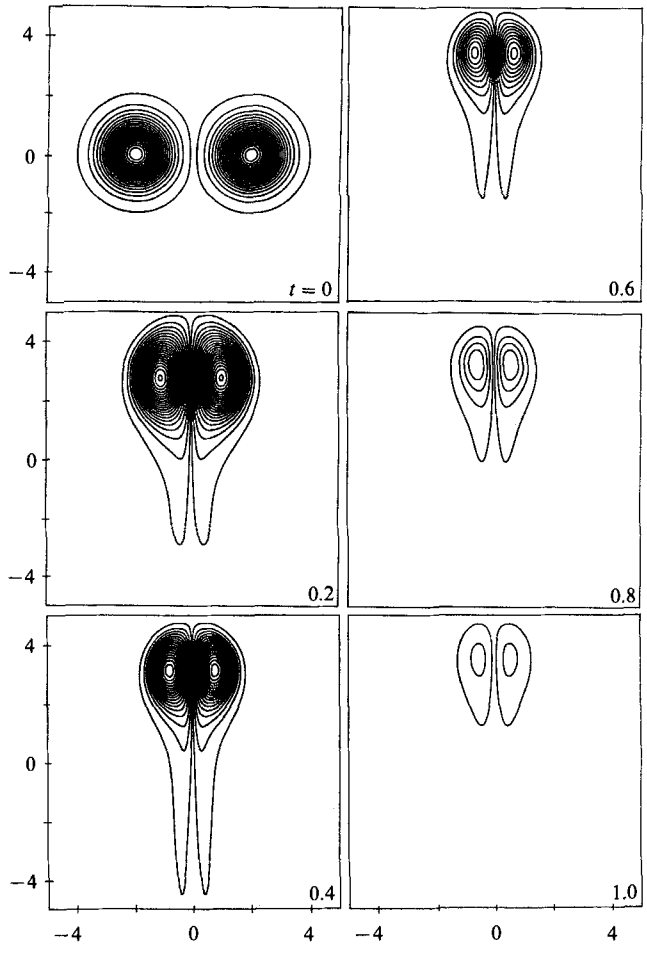

FIGURE 15. Cancellation of two opposite-signed vortices in a non-axisymmetric strain field, $\gamma = 4$, $\beta = 4$, $Re = \Gamma_0/2\pi\nu = 160$. The minimum contour is $|\omega_{\min}| = 5$ and all contour intervals are $|\Delta\omega| = 15$.

and 18. The first frame in each of these figures shows how the circulation in a half-plane for each pair varied with time (the total circulation was always zero). Figure 17 shows the cancellation behaviour for two Burgers vortices to be independent of Re at fixed $\beta = 2$ in the calculated range $0.1 \geqslant Re \geqslant 160$. Strong dependence on β was found. The extreme vortex elongation induced by the y-component of the strain at large β with γ fixed (e.g. figure 16) suggests that when $\beta \gg 1$ the cancellation event may be modelled by approximating the vortices by shear layers with vorticity $\omega = \omega(x, t)$ uniform in the y-direction. The vorticity transport equation may then be reduced to the one-dimensional heat equation by the transformation

$$B(t) = \int_0^t \beta(t')\,\mathrm{d}t', \tag{5.6}$$

$$\xi = x\,\mathrm{e}^{B(t)}, \tag{5.7}$$

$$\tau = \int_0^t \mathrm{e}^{2B(t')}\,\mathrm{d}t', \tag{5.8}$$

$$\Omega(\xi, \tau) = \omega(x, t)\,\mathrm{e}^{-A(t)}, \tag{5.9}$$

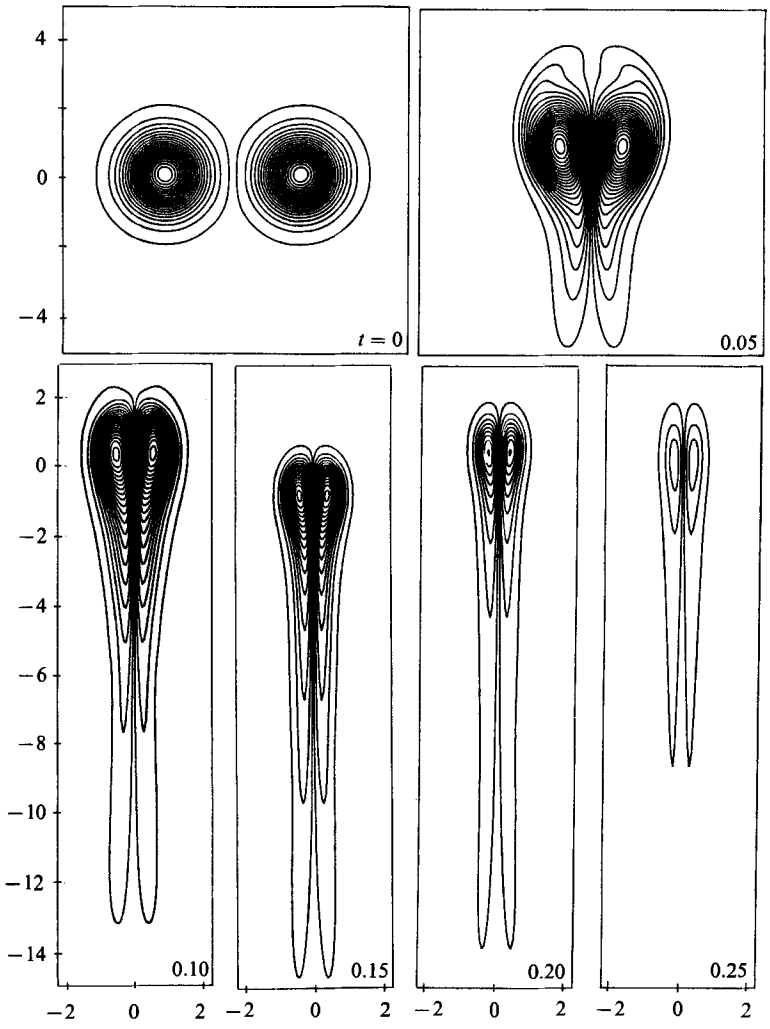

FIGURE 16. Cancellation of two opposite-signed vortices in a non-axisymmetric strain field, $\gamma = 4$, $\beta = 16$, $Re = \Gamma_0/2\pi\nu = 160$. The minimum contour is $|\omega_{\min}| = 5$ and all contour intervals are $|\Delta\omega| = 15$.

where $A(t)$ is given by (2.21). Returning to dimensional coordinates and discarding the 'overbars' notation for dimensional variables, let $\omega_0(x), \omega_0(-x) = -\omega_0(x)$ be the initial ω-distribution for the double shear layer. An analytic solution for this flow in the presence of a strain field like (2.4) has been given by Kambe (1984) as

$$\omega(x,t) = \frac{\mathrm{e}^{A(t)}}{[4\pi\nu\tau(t)]^{\frac{1}{2}}} \int_{-\infty}^{\infty} \omega_0(x') \exp\left[-\frac{(\mathrm{e}^{B(t)}x - x')^2}{4\nu\tau(t)}\right] \mathrm{d}x'. \tag{5.10}$$

We consider a strip of shear layer of initially unit length in the y-direction. Assuming constant β and γ with $\beta > 0$, accounting for the y-stretching of the strip by a factor $\exp[(\beta-\gamma)t]$ in time t, and approximating

$$\int_{-\infty}^{\infty} x'\omega_0(x')\,\mathrm{d}x' \approx 2x_0\Gamma_0,$$

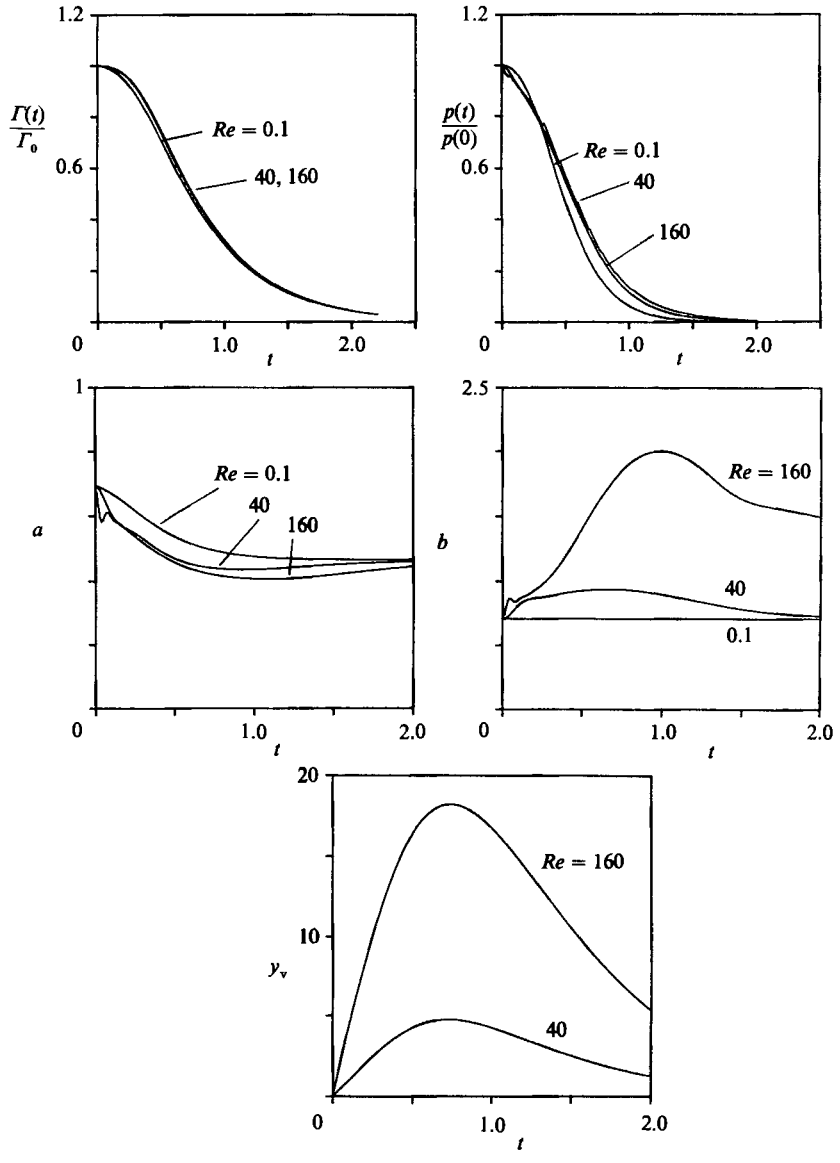

FIGURE 17. Flow diagnostics for the cancellation events where $\beta = 2$, $Re = 0.1, 40, 160$.

where x_0 is the initial shear-layer centroid, the circulation in the strip is asymptotically, when $\beta t \gg 1$,

$$\Gamma(t) \sim \Gamma_0 x_0 \left(\frac{2\beta}{\pi\nu}\right)^{\frac{1}{2}} e^{-\beta t} + O(e^{-2\beta t}). \tag{5.11}$$

There is complete vorticity cancellation as $t \to \infty$ when $\beta > 0$. If $\beta < 0$ the strain attenuates cancellation by convecting vorticity away from $x = 0$. When $t \to \infty$ the residual circulation in $x > 0$ is then given by

$$\Gamma(\infty) = \int_0^\infty \omega_0(x') \operatorname{erf}\left[\left(\frac{|\beta|}{2\nu}\right)^{\frac{1}{2}} x'\right] dx'. \tag{5.12}$$

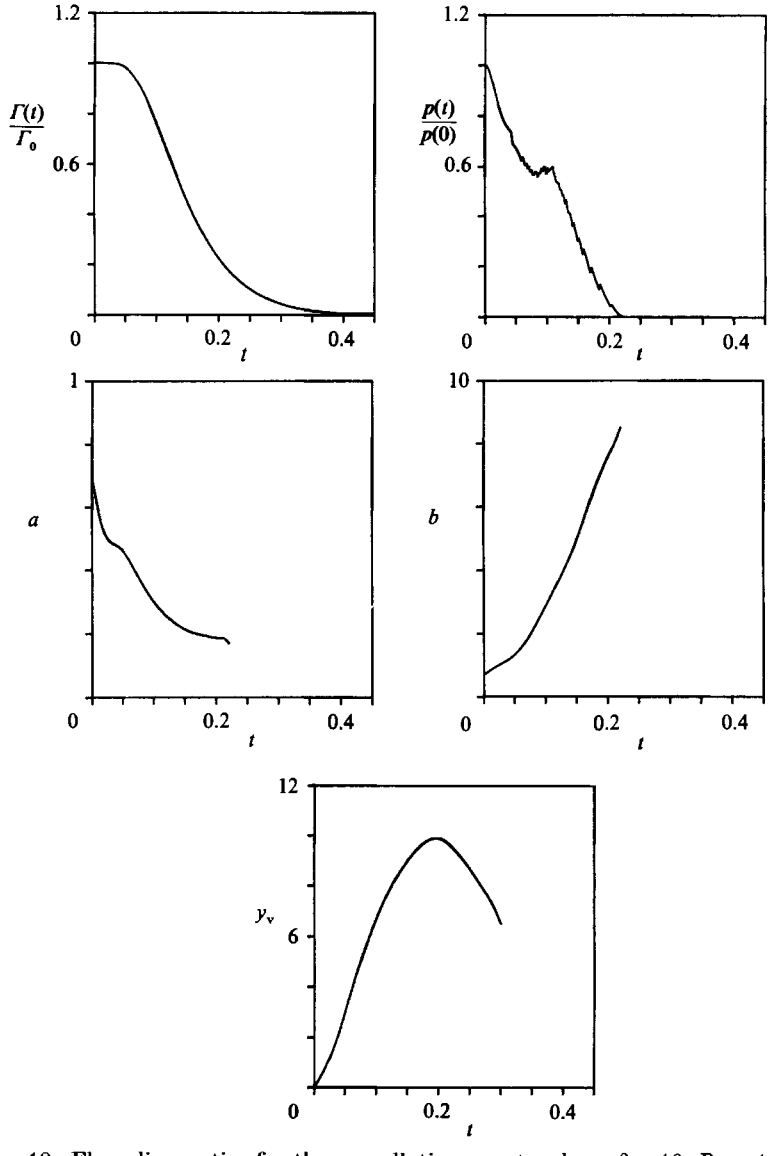

FIGURE 18. Flow diagnostics for the cancellation events where $\beta = 16$, $Re = 160$.

We note that (5.11) and (5.12) are independent of γ: straining in the direction of the vortex lines does not *per se* influence (asymptotically) vorticity cancellation. After non-dimensionalization and setting $x_0 = 2$, equation (5.11) is shown plotted in figure 19 along with the current cancellation results for Burgers vortices ($\gamma = 4, \beta = 2, 4, 8,$ 16). In all cases $Re = 160$. There is reasonable agreement even when $\beta = \frac{1}{2}\gamma = 2$ and the vortices are not sheet-like.

Schatzle (1987) studied experimentally the collision between two vortex rings leading to vortex reconnection. Schatzle's figure 6.12 shows the decrease of circulation for each of the cores at the contact site, where a rapid cancellation of circulation for the two vortex rings occurs (taking a cut locally through the cores, the vorticity distributions are of opposite sign). Schatzle measures large rates of strain during the vortex cancellation event. Although the strain rates vary, a representative

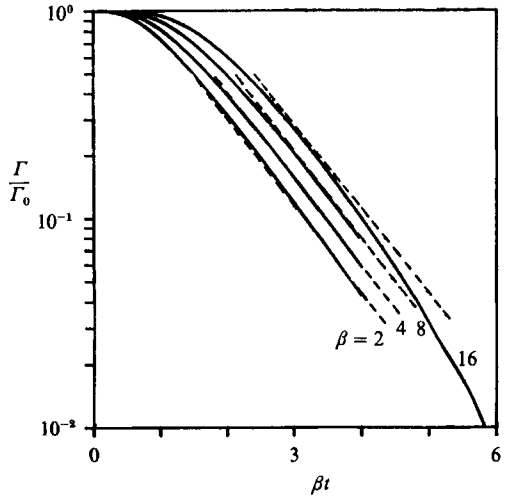

FIGURE 19. Circulation Γ versus βt: ——, present; – – – –, from Kambe (1984).

value of β is 6 s^{-1} (his figure 6.6). From (5.11) and using $\nu = 0.01$ cm^2 s^{-1} (water) and $x_0 = 0.5$ cm, the time for the circulation to drop to 10% of its original value ($\Gamma/\Gamma_0 = 0.1$), is $t_{10} = 0.9$ s. From Schatzle's figure 6.12, the observed time is of order 1 s. We note that in the experiment, β exhibits both a temporal and a strong spatial variation which results from the three-dimensional dynamics of the reconnection/cancellation event. This has not been modelled here, but appears to be a central issue in the vortex reconnection phenomenon.

5.4. *Time-varying strain*

Our results can elucidate certain vortex flows with uniform but time-varying strain. Specifically, consider a flow with two-dimensional space, time and vorticity variables $(\hat{x}, \hat{t}, \hat{\omega}(\hat{x}, \hat{t}))$ embbeded in a strain field (2.8) with non-constant strain rates

$$\hat{\gamma} = a_1/(t_0 - \hat{t}), \tag{5.13}$$

$$\hat{\beta} = b_1/(t_0 - \hat{t}), \tag{5.14}$$

where a_1, b_1 are constants and t_0 is a critical time. When $a_1 > 0$ there is infinite stretching of vortex lines as $l = l_0 t_0^{a_1}/(t_0 - \hat{t})^{a_1}$ when $\hat{t} \to t_0$ from below.

The transformation

$$\boldsymbol{x} = \hat{\boldsymbol{x}}\left(\frac{t_0}{t_0 - \hat{t}}\right)^{\frac{1}{2}}, \tag{5.15}$$

$$t = t_0 \ln\left(\frac{t_0}{t_0 - \hat{t}}\right), \tag{5.16}$$

$$\omega = \hat{\omega}\left(\frac{t_0 - \hat{t}}{t_0}\right), \tag{5.17}$$

maps the $(\hat{x}, \hat{t}, \hat{\omega})$-flow into a flow with corresponding variables $(\boldsymbol{x}, t, \omega)$ and with constant strain rates

$$\gamma = (a_1 - 1)/t_0, \tag{5.18}$$

$$\beta = (b_1 - \tfrac{1}{2})/t_0. \tag{5.19}$$

The $(\boldsymbol{x}, t, \omega)$-flow is that studied here.

Siggia & Pumir (1988) performed a three-dimensional Biot–Savart simulation of a vortex tube with circular core of cross-sectional area assumed inversely proportional to the local stretching of vortex lines. Their results show vortex-dipole formation and suggest pointwise collapse to infinite stretching in a finite time with vorticity-aligned strain like (5.13). For vortex-pair initial conditions (5.5) our results support (5.11) for the asymptotic $(\boldsymbol{x}, t, \omega)$-flow when $\beta > 0$. This is not conclusive since our numerics do not span the whole (γ, β)-plane, but the argument is strengthened if also $\beta - \gamma > 0$, in which case each core will not remain nearly circular but the pair will tend to flatten into the elongated dipole as in figure 16. Given (5.11), it follows from (5.15)–(5.19) that there will be complete vortex cancellation in the $(\hat{\boldsymbol{x}}, \hat{t}, \hat{\omega})$-flow when $\hat{t} \to t_0$ provided $b_1 > \frac{1}{2}$, independent of a_1 (i.e. $\hat{\gamma}$). This will suppress the incipient inviscid singularity implied by (5.13): see also Meiron *et al.* (1988). The numerics of Siggia & Pumir indicate $a_1 = 1 + \log$ terms for the vortex-tube evolution: b_1 is not given explicitly but Siggia & Pumir assume $b_1 = \frac{1}{2}a_1$ (axisymmetric strain) and here the hypothesis can be proven rigorously by a further transformation of the $(\boldsymbol{x}, t, \omega)$-flow to an unstrained flow (§2.3). The essential result is that viscous cancellation and hence singularity suppression is controlled by b_1 alone.

5.5. *Vortex dimensions and pressure*

Vortex dimensions were defined using

$$a^2 = \frac{4 \int_A (x - x_{\text{mean}})^2 \omega \, \mathrm{d}A}{\int_A \omega \, \mathrm{d}A}, \tag{5.20}$$

$$b^2 = \frac{4 \int_A (y - y_{\text{mean}})^2 \omega \, \mathrm{d}A}{\int_A \omega \, \mathrm{d}A}, \tag{5.21}$$

where A is the left half-plane $x < 0$. For uniform vorticity in an elliptical region and zero vorticity outside, a and b are the ellipse semi-major and -minor axes. As the vortices came together, their aspect ratio a/b decreased. Several of these calculations were halted before the cancellation had nearly completed owing to inaccuracies in computing a, when low-level oscillations in ω appeared at large $|r|$. These were associated with the limit of circumferential resolution when, at late time, and with large β, the vortex-tail thickness was of order the circumferential grid spacing (e.g. figure 16).

The distance that the vortex centroids moved vertically away from their initial position is given in the plot of y_{v} versus time (figures 17 and 18), where

$$y_{\text{v}} = y_{\text{c}} + y_{\text{mean}}. \tag{5.22}$$

In (5.22) y_{c} is given by (5.4) and y_{mean} is the y-centroid, located with respect to the moving axes. Although v_{c} is estimated and used as the velocity at which the reference axes move, the vortex centroids tend to drift relative to these axes; y_{mean} measures this drift.

The vortex core pressure p_{c} is defined as the pressure at a grid point nearest the

vorticity extremum. This can be calculated either by solving an appropriate Poisson equation or, as is done here, by using the radial momentum equation,

$$\begin{aligned}\frac{1}{\rho}\frac{\partial p^*}{\partial r} = \nu\left\{\frac{\partial^2 v_r}{\partial r^2}+\frac{1}{r}\frac{\partial v_r}{\partial r}+\frac{1}{r^2}\frac{\partial^2 v_r}{\partial\theta^2}-\frac{1}{r^2}v_r-\frac{2}{r^2}\frac{\partial v_\theta}{\partial\theta}\right\}\\ +\frac{v_\theta^2}{r}-v_r\frac{\partial v_r}{\partial r}-\frac{v_\theta}{r}\frac{\partial v_r}{\partial\theta}-\frac{\partial v_r}{\partial t}+\tfrac{1}{2}\gamma v_r\\ -\frac{v_\theta}{r}y_c(\beta-\gamma)\cos\theta+\tfrac{1}{2}(2\beta-\gamma)\cos 2\theta\, v_r\\ +[\tfrac{1}{2}r\{(2\beta-\gamma)\cos 2\theta+\gamma\}+y_c(\beta-\gamma)\sin\theta]\frac{\partial v_r}{\partial r}\\ -\left[\tfrac{1}{2}\{(2\beta-\gamma)\sin 2\theta+\gamma\}-\frac{y_c}{r}(\beta-\gamma)\cos\theta\right]\frac{\partial v_r}{\partial\theta}.\end{aligned} \tag{5.23}$$

In (5.23), $p^* = p - p_s, p$ is the pressure at a general point in the flow, $p_s = -\frac{1}{2}\rho[\beta^2x^2+(\beta-\gamma)^2y^2]$ is the pressure due to the strain field alone and ρ is the density. p_c^* was calculated by integrating (5.23) along a radial line from $r = \infty$ to the centre of the vortex core. At $r\to\infty$ the θ-momentum equation gives

$$p^*(r\to\infty,\theta) = -\frac{\rho\Gamma}{4\pi}(2\beta-\gamma)\sin 2\theta. \tag{5.24}$$

When the total circulation Γ is non-zero this must be used as a boundary condition on p^* at $r\to\infty$ to ensure that the computed pressure is independent of the path of integration. Since the core pressure was not calculated at the true ω-extremum, but at the nearest grid point, there was some fluctuation in the calculated p_c caused by discontinuous jumps in the selected grid-point position. This can be seen for example in figure 18.

Moore & Saffman (1971) calculated the shape of steady finite-area vortices with uniform vorticity ω in an inviscid fluid under an applied two-dimensional, irrotational strain field. Stable vortices were found if the ratio of the applied strain to the vorticity was less than 0.15. The vortices were elliptical with the ellipse principal axes aligned at 45° to those of the strain field. The pressure at the vortex centre can be calculated using the Bernoulli equation for a rotational fluid with constant vorticity, with the result (P. G. Saffman; private communication)

$$\frac{p_c}{\rho} = \frac{-\omega^2a^2b^2}{2(a^2+b^2)}, \tag{5.25}$$

where a and b are the vortex semi-major and -minor axes respectively. At the vortex centre, $p_s = 0$. To test (5.25) when applied to viscous, unsteady, non-discrete vortices, calculated $P = p_c^*/\rho$ were plotted using $Re = 160$ cancellation data for the $\beta = 4, 8, 16$ cases. The results are shown in figure 20 where ω is estimated as $\omega = \max_{i,j}|\omega(i,j)|$, the vorticity at the grid point with the largest magnitude of vorticity. This gives good agreement with (5.25). The pressure calculations that deviate most from the model are from the $Re = 160, \beta = 16$ event, which showed pressure fluctuation during its decay, for reasons discussed previously.

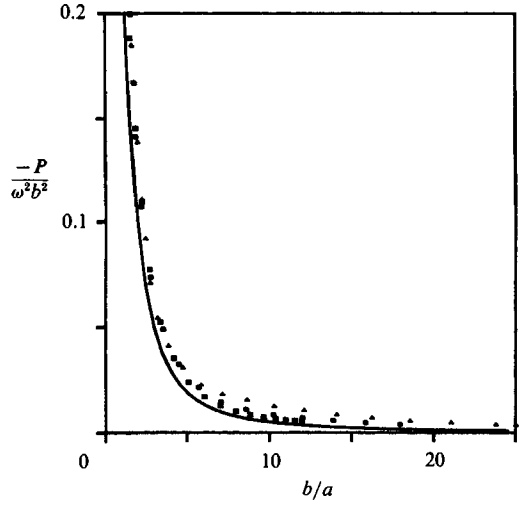

FIGURE 20. Vortex pressure: ——, from Moore & Saffman (1971). Present results from cancelling vortices at $Re = 160$; ■, $\beta = 4$; ●, $\beta = 8$; ▲, $\beta = 16$. ω is taken as $\max_{i,j}|\omega(i,j)|$.

6. Conclusion

The merging of two Burgers vortices was studied for Reynolds numbers in the range $Re = \Gamma/2\pi\nu = 10$–1280. Convective effects were found to become more dominant as the Reynolds number increased. This was expected since the strength of viscosity and the strain intensification were fixed in the scaling adopted. Axisymmetrization of the vorticity distribution occurred over a time consistent with the convection timescale. Initial vortex separation was found to affect little the qualitative behaviour of a merging event.

The results of the higher-Reynolds-number merging simulations were used to model the energy spectrum for homogeneous turbulence. At lower wavenumber the behaviour of the spectrum was found to be like k^{-1} – a result of the Burgers-vortex basis of the model – while the highest wavenumber range ($k/k_d > 1$) agreed well with Heisenberg's k^{-7} law without the constraint that eddies on different scales be statistically independent. An unresolved region remains in the energy spectra for the two highest Reynolds number merging events ($Re = 640, 1280$).

Cancellation of two opposite-signed Burgers vortices over the Reynolds-number range $Re = 0.1$–160 was also studied. For a constant value of the strain β in the direction joining the vortex centroids, the circulation about one vortex was found to decay approximately as $\beta^{\frac{1}{2}}\exp(-\beta t)$, independent of Reynolds number, in good agreement with an approximation based on Kambe's (1984) solution describing the strain-induced collision of two vortex layers. The cancellation timescale is consistent with Schatzle's (1987) measurements of strain-enhanced vortex cancellation during the collision between two vortex rings when a typical value of β is used, although we emphasize that Schatzle's measured strain rates are not constant over the decay period. Calculated vortex-core pressures showed good agreement with a simple analytical result obtained from the inviscid uniform-vorticity model of Moore & Saffman (1971).

Finally, since the dynamics of vortices embedded in an axisymmetric strain field can be mapped onto an equivalent two-dimensional flow without strain (§2.3), the present results for the merging and cancellation events are relevant to the evolution

of any flow with a similar initial vorticity field but with time-dependent axisymmetric strain $\beta(t) = \frac{1}{2}\gamma(t)$. The investigation of specific time-varying strain scenarios is one area for future study.

Helpful discussions with Dr P. A. Jacobs and Professor P. G. Saffman are gratefully acknowledged. This work was supported by the Australian Research Council under grant number A48315031.

REFERENCES

ASHURST, W. T., KERSTEIN, A. R., KERR, R. M. & GIBSON, C. H. 1987 Alignment of vorticity and scalar gradient with strain rate in simulated Navier–Stokes turbulence. *Phys. Fluids* **30**, 2343–2353.

BATCHELOR, G. K. 1967 *An Introduction to Fluid Mechanics*. Cambridge University Press.

BURGERS, J. M. 1948 A mathematical model illustrating the theory of turbulence. *Adv. Appl. Mech.* **1**, 171–199.

CORCOS, G. M. & LIN, S. J. 1984 The mixing layer: deterministic models of a turbulent flow. Part 2. The origin of three-dimensional motion. *J. Fluid Mech.* **139**, 67–96.

CORCOS, G. M. & SHERMAN, F. S. 1984 The mixing layer: deterministic models of a turbulent flow. Part 1. Introduction and the two dimensional flow. *J. Fluid Mech.* **139**, 29–65.

DEEM, G. S. & ZABUSKY, N. J. 1978 Stationary V-states: interactions, recurrence and breaking. *Phys. Rev. Lett.* **40**, 859.

GIGA, Y. & KAMBE, T. 1987 Large time behaviour of the vorticity of two dimensional viscous flow and vortex formation in three-dimensional flow. *IUTAM Symp. on Fundamental Aspects of Vortex Motion, Tokyo, Japan.*

HINZE, J. O. 1975 *Turbulence*, 2nd edn. McGraw-Hill.

JACOBS, P. A. 1987 Nonlinear dynamics of piecewise-constant vorticity distributions in an inviscid fluid. Ph.D. thesis, University of Queensland.

JACOBS, P. A. & PULLIN, D. I. 1985 Coalescence of stretching vortices. *Phys. Fluids* **28**, 1619–1625.

KAMBE, T. 1984 Some dissipation mechanisms in vortex systems. In *Turbulence and Chaotic Phenomena* (ed. T. Tatsumo), pp. 239–244. *IUTAM.*

KIDA, S. 1981 Motion of an elliptic vortex in a uniform shear flow. *J. Phys. Soc. Japan* **50**, 3157.

LEONARD, A. & WINCKLEMANS, G. 1988 Improved vortex methods for three-dimensional flows with applications to the interactions of two vortex rings. *SIAM Workshop on Mathematical Aspects of Vortex Dynamics, Leesburg Virginia, April 25–28.*

LIN, S. J. & CORCOS, G. M. 1984 The mixing layer: deterministic models of a turbulent flow. Part 3. The effect of plane strain on the dynamics of streamwise vortices. *J. Fluid Mech.* **141**, 139–178.

LUNDGREN, T. S. 1982 Strained spiral vortex model for turbulent fine structure. *Phys. Fluids* **25**, 2193–2203.

MEIRON, D. I., ORSZAG, S. A. & SHELLY, M. J. 1988 A numerical study of vortex reconnection. *SIAM Workshop on Mathematical Aspects of Vortex Dynamics, Leesburg, Virginia, April 25–28.*

MELANDER, M. V., MCWILLIAMS, J. C. & ZABUSKY, N. J. 1987 Axisymmetrization and vorticity-gradient intensification of an isolated two-dimensional vortex through filamentation. *J. Fluid Mech.* **178**, 137–159.

MELANDER, M. V., ZABUSKY, N. J. & MCWILLIAMS, J. C. 1988 Symmetric vortex merger in two dimensions: causes and conditions. *J. Fluid Mech.* **195**, 303–340.

MOORE, D. W. & SAFFMAN, P. G. 1971 Structure of a line vortex in an imposed strain. In *Aircraft Wake Turbulence* (ed. J. Olsen, A. Goldberg & N. Rogers), pp. 339–354. Plenum.

NEU, J. C. 1984*a* The dynamics of a columnar vortex in an imposed strain. *Phys. Fluids* **27**, 2397–2402.

NEU, J. C. 1984*b* The dynamics of stretched vortices. *J. Fluid Mech.* **143**, 253–276.

PEACE, A. J. & RILEY, N. 1983 A viscous vortex pair in ground effect. *J. Fluid Mech.* **129**, 409–426.

PERRY, A. E. & CHONG, M. S. 1982 On the mechanism of wall turbulence. *J. Fluid Mech.* **119**, 173–218.

ROBINSON, A. C. & SAFFMAN, P. G. 1984 Stability and structure of stretched vortices. *Stud. Appl. Maths* **70**, 163–181.

SCHATZLE, P. R. 1987 An experimental study of fusion of vortex rings. Ph.D. thesis, California Institute of Technology.

SIGGIA, E. D. & PUMIR, A. 1988 Incipient singularities in the Navier–Stokes equations. Preprint, Cornel University.

TOWNSEND, A. A. 1951 On the fine-scale structure of turbulence. *Proc. R. Soc. Lond.* A **208**, 534–542.